《工程科学学报》编辑部

电渣重熔易氧化元素控制的研究进展

段生朝，张立峰✉

北方工业大学 机械与材料工程学院 北京 100144

✉ 通信作者，E-mail: zhanglifeng@ncut.edu.cn

摘　要　电渣重熔是重要的二次精炼技术，不仅可以去除钢中杂质元素和非金属夹杂物，还可以改善铸锭的凝固组织进而提升钢的力学性能。若钢中含有易氧化合金元素，如 Al、Ti、Si、B 和稀土元素，会与 CaF_2-CaO-Al_2O_3 基重熔渣系中的不稳定组元发生化学反应，造成合金元素沿铸锭高度方向分布不均匀现象。为抑制电渣重熔过程易氧化元素的烧损，在电渣重熔温度范围内，分析 CaF_2-CaO-Al_2O_3 基重熔渣系中各个组元对钢中目标控制元素含量的影响可以实现重熔渣系成分的准确设计，这取决于渣相和合金相中组元活度的准确计算。除了在重熔渣系中添加对应元素的氧化物之外，CaF_2-CaO-Al_2O_3 基重熔渣系中公共组元 CaO 和 Al_2O_3 以及温度对钢中不同合金元素含量的影响也并不相同。电渣重熔过程传质模型预报结果的准确性依赖于熔渣和钢液中组元的热力学活度、不同反应位置温度（电极端部、金属熔滴、渣池和金属熔池界面）、传质系数和几何参数的准确估计，但不同电渣重熔操作、重熔渣系成分和钢种对以上参数都有较大影响。由于准确估计不同反应位置处的反应温度和流体流动对传质系数的影响比较困难，因此相比较热力学分析，易氧化元素反应的动力学研究仍比较匮乏。重熔渣系物性参数对铸锭的表面和凝固质量同样有重要影响，目前对含 TiO_2、SiO_2、B_2O_3 和稀土氧化物的重熔渣系的物性参数研究主要集中在黏度和结晶能力等方面，但对其活度的实验室研究还未见报道。低氟重熔渣系的开发越来越受到关注，针对低氟重熔渣系条件下钢中易氧化元素控制的热力学、动力学和熔渣物性参数研究还有待于进一步开展。

关键词　电渣重熔；热力学；动力学；渣系设计；物性参数

分类号　TF141

Research progress on the control of reactive elements in remelted ingots during electroslag remelting process

DUAN Sheng-chao, ZHANG Li-feng ✉

School of Mechanical and Materials Engineering, North China University of Technology, Beijing 100144, China

✉ Corresponding author, E-mail: zhanglifeng@ncut.edu.cn

ABSTRACT　Electroslag remelting (ESR) is an important secondary refining technique capable of removing impurity elements and non-metallic inclusions, improving the solidification structure of the ingots, and enhancing the mechanical properties of the steels. When steels contain easily oxidizable alloying elements such as Al, Ti, Si, B, and rare earth elements (REEs), the strong chemical reactions between the alloying elements and the unstable components in the CaF_2-CaO-Al_2O_3-based ESR type slag system occur in the slag/metal interface, leading to the non-uniform distribution of the alloying elements along the height of the remelted ingots and the deterioration of mechanical properties of the steels. To mitigate the oxidation loss of these alloying elements during the ESR process, precise design of the composition of the CaF_2-CaO-Al_2O_3-based ESR type slag system enables accurate control of the reactive alloying elements within their target composition range, which relies on the feasibility of the calculated thermodynamic activities of components in the slag and alloys employing ion-molecular

基金项目：国家重点研发计划(2023YFB3709900)、国家自然科学基金(U22A20171，52404335)

coexistence theory and Wagner equation, respectively. Apart from incorporating corresponding oxide additives into the ESR-type slag system to prevent the oxidation loss of the alloying element in the electrode during the ESR process, the effects of common components like CaO and Al_2O_3 in the ESR-type slag as well as temperature on the different alloying element contents are different. For instance, the control of Al and Ti contents in alloys depends on the combined effects of the composition range of CaO and remelting temperature besides the Al_2O_3 in the ESR-type slag. For the B-bearing steels, the B content in alloys can be controlled by CaO content rather than Al_2O_3. In the case of alloys containing rare earth elements, *i.e.*, La, Ce, and Y, the addition of CaO can improve the yield rate of the rare earth elements, while the addition of Al_2O_3 has a negative effect. The accuracy of mass transfer models during ESR depends on not only the precise estimation of thermodynamic activities of components in both slag and molten steel, but also temperatures at different reaction locations (electrode tip, metal droplet, interface between slag bath and metal pool), mass transfer coefficients, and geometric parameters. However, these parameters above are significantly influenced by different ESR operations, slag compositions, and steel grades, etc. Due to the difficulty in determining reaction temperatures and fluid flow in the ESR furnace, therefore the mass transfer coefficients of relative elements in both slag and metal phases at different reaction locations can not be precisely estimated. Thus, the kinetic studies of the reactive elements remain relatively scarce compared to thermodynamic analyses. Physical parameters of the slag system also critically affect the surface and solidification quality of ingots. Current research on the physical parameters of remelting slag systems containing TiO_2, SiO_2, B_2O_3, and rare earth oxides mainly focuses on viscosity and crystallization ability, while laboratory studies on their activities are yet to be reported up to now. The development of low-fluorine ESR-type slag systems attracts more attention, therefore the relative fundamental research, *viz*., thermodynamics and physicochemical properties of the low-fluorine slag, on the control of the reactive alloying element contents in the ESR remelted ingots is very necessary.

KEY WORDS Electroslag remelting; Thermodynamics; Kinetics; Slag composition design; Physic property

电渣重熔（Electroslag remelting, ESR）是一种重要的二次精炼工艺，熔渣在自耗电极重熔过程将电能转换为热能，电极端部形成的液膜不断聚集形成液滴，随后滴落穿过液态渣层进入到金属熔池，在水冷结晶器中逐渐凝固成为电渣锭[1, 2]。自耗电极通过电渣重熔精炼后可以进一步去除钢中杂质元素和非金属夹杂物[3-5]。同时由于水冷结晶器的作用，可以提高钢液的凝固速率，改善铸锭的凝固组织结构，进而使钢的力学性能得到较大提升[6-8]。但是，另一方面，重熔渣系 CaF_2-CaO-Al_2O_3 中存在的不稳定组元，如 Al_2O_3、TiO_2 和 SiO_2，给电渣锭中易氧化元素（Al、Ti、Si 和 B）的控制也带来一定的困难[9-11]。电渣重熔过程中熔渣与合金体系处于一个动态变化的过程，特别是升温阶段，其稳定性的控制变得尤为困难，因此导致在大多数情况下很难保证电渣锭中易氧化元素的均匀化控制，致使其力学性能大幅降低。

为了减少电渣重熔铸锭中易氧化元素损失，通常是向熔渣中加入一定量的对应烧损元素的氧化物，使得该氧化反应达到热力学平衡，进而限制反应朝着形成金属氧化物方向进行。使用上述方法通常存在以下几个问题[12, 13]：（1）不同的氧化物 M_xO_y（M = Al、Ti、Si 和 B 等）存在不同的化学平衡，从而所添加的相应的氧化物是否可以起到抑制氧化反应的作用，即针对不同氧化反应所添加的氧化物的量应不一致；（2）过量添加特定氧化物会改变电渣重熔渣系的物理化学性质，例如融化温度、粘度、电导率和表面张力等均取决于熔渣的组成[14, 15]。另一种方法是设计自耗电极中某种易氧化元素的含量超出其标准成分范围的上限，电渣重熔过程中再控制在标准的成分范围内，但这种方法会导致额外的制造成本[12]。对于不同电渣重熔工艺，如液态电渣连铸[16]、电渣快速重熔[17]

和抽锭式电渣重熔[18]，和电渣重熔铁基或镍基合金时所用的渣系成分并不相同。加之电渣重熔过程中渣池及渣/金界面温度分布受工艺参数的影响且很难通过实验准确测量[19-21]，这对渣系成分合理设计以及电渣锭中易氧化元素的均匀化控制造成很大困难。陈崇禧等人[22]因此建立了镍基合金中 Mg、Al 和 Ti 含量与熔渣 CaF_2-MgO-Al_2O_3-CaO-TiO_2 成分和电极融化速率及熔池渣界面积的数学关系以研究渣系对合金元素烧损的影响规律。显然，该方法存在一定的局限性不能够适应不同电渣重熔工艺和钢种对易氧化元素均匀化控制的要求。因此，通过渣系成分的合理设计实现电渣锭中易氧化元素的精准控制就显得十分重要。本文将对电渣重熔铁、镍基合金中不同种类易氧化元素烧损的热力学、动力学及重熔渣系物性参数的相关研究进行了总结，为电渣重熔制备高品质特殊钢提供理论基础。

1 电渣重熔过程易氧化元素控制的热力学

1.1 电渣重熔含 Al、Ti 合金渣系成分设计

1968 年德国埃德尔特钢厂（Edelstahlwerk Witten AG）在电渣重熔含钛不锈钢、耐热钢和热作模具钢时发现（最大电流 18 kA，电压 25 ~ 100 V，熔速 500 $kg\cdot h^{-1}$，40%CaO-40%Al_2O_3-20%CaF_2），自耗电极中 Al、Ti 和 Si 元素含量容易发生氧化使得电渣锭中这些合金元素沿铸锭高度方向分布不均匀。特别是在电渣锭底部位置（即电渣重熔开始阶段）Ti 和 Si 元素烧损较为严重，然而电极中 Al 元素含量较高时，电渣锭中 Al 元素轻微烧损，但当电极中 Al 元素含量较低时，电渣锭中 Al 元素出现增加现象[23]。Pateisky 等人[23]解释出现上述现象的原因可能是：一方面电极表面的氧化层造成熔渣高氧势和大气中的氧参与氧化反应，另一方面渣中不稳定组元 Al_2O_3、TiO_2 和 SiO_2 与 Al、Ti 和 Si 元素间的氧化还原反应造成烧损，如下式所示。

$$3[Ti]+2(Al_2O_3)=4[Al]+3(TiO_2)$$

$$\lg K_1=\lg\frac{a_{\%,Al}^4\cdot a_{R,TiO_2}^3}{a_{\%,Ti}^3\cdot a_{R,Al_2O_3}^2}=\lg\frac{f_{\%,Al}^4\cdot[\%Al]^4\cdot\gamma_{TiO_2}^3\cdot X_{TiO_2}^3}{f_{\%,Ti}^3\cdot[\%Ti]^3\cdot\gamma_{Al_2O_3}^2\cdot X_{Al_2O_3}^2}=-\frac{35300}{T}+9.94 \tag{1}$$

$$4[Al]+3(SiO_2)=3[Si]+2(Al_2O_3)$$

$$\lg K_2=\lg\frac{a_{\%,Si}^3\cdot a_{R,Al_2O_3}^2}{a_{\%,Al}^4\cdot a_{R,SiO_2}^3}=\lg\frac{f_{\%,Si}^3\cdot[\%Si]^3\cdot\gamma_{Al_2O_3}^2\cdot X_{Al_2O_3}^2}{f_{\%,Al}^4\cdot[\%Al]^4\cdot\gamma_{SiO_2}^3\cdot X_{SiO_2}^3}=\frac{35840}{T}-5.86 \tag{2}$$

$$[Ti]+(SiO_2)=[Si]+(TiO_2)$$

$$\lg K_3=\lg\frac{a_{\%,Si}\cdot a_{R,TiO_2}}{a_{\%,Ti}\cdot a_{R,SiO_2}}=\lg\frac{f_{\%,Si}\cdot[\%Si]\cdot\gamma_{TiO_2}\cdot X_{TiO_2}}{f_{\%,Ti}\cdot[\%Ti]\cdot\gamma_{SiO_2}\cdot X_{SiO_2}}=\frac{180}{T}+1.36 \tag{3}$$

式中，K_i 为反应的平衡常数；$a_{\%,i}$ 和 $a_{R,i}$ 分别为合金熔体中组元 i 以百分之一溶液为标准态和熔渣组元 i 以纯物质未标准态的活度；$f_{\%,i}$ 和 γ_i 分别合金熔体中组元 i 以百分之一溶液为标准态的活度系数和熔渣组元 i 以纯物质未标准态的活度系数；[%i]和 X_i 分别是合金熔体中和熔渣组元 i 的质量百分浓度和摩尔分数。

如上所述，重熔过程渣系成分对电渣锭中易氧化元素的均匀化控制具有重要影响，而这主要依

赖于 CaF_2-CaO-Al_2O_3 基渣系中各个组元和合金熔体中活度计算的准确性[24]。对于电渣重熔渣系组元活度的计算，国内学者大多使用离子-分子共存理论（Ion and molecular coexistence theory, IMCT）计算重熔渣系的热力学活度[25-28]，其计算的准确度也逐渐受到国外学者的广泛认可[26]。冶炼温度下合金熔体中组元的活度系数 $f_{\%,i}$ 则使用 Wagner 模型[29]计算，如式（4）所示。

$$\lg f_{\%,i} = \sum e_i^j [\%j] \tag{4}$$

式中：e_i^j 为一阶相互作用系数。目前绝大部分研究者在计算铁基和镍基合金中组元活度系数时，选用铁液中的一阶相互作用系数[11, 25, 30, 31]。Shen 等人[30]在制备大型 GH4706 电渣锭（直径 1100 mm）时进行渣系成分设计时发现，使用瓦格纳模型计算镍基高温合金中 Al 和 Ti 的活度系数时，可以忽略 Ni 元素的情况下使用铁液中的活度相互作用系数也可以达到满意的结果。

由于钛的氧化物 TiO_x 中钛离子可以在渣中以多种价态形式存在，陈崇禧[32]等人认为与合金中 Ti 相平衡的渣中低价钛氧化物是 Ti_3O_5，降低 Ti^{3+}向气/渣界面扩散速率是控制合金中 Ti 元素烧损的关键。Yang 等人[33]使用 X 射线光电子能谱（X-ray photoelectron spectroscopy, XPS）测量了 CaF_2-CaO-Al_2O_3-MgO-(5 ~ 30 wt.%)TiO_2 渣系中钛离子的价态，结果表明无论渣中 TiO_2 含量如何钛离子都主要以 Ti^{4+}的形式存在，这意味着渣中钛的氧化物 TiO_x 可以被近似地认为全部为 TiO_2 并计算其活度。通过使用 IMCT 和 Wagner 模型分别获得熔渣和金属熔体的热力学活度后，Jiang 等人[25]通过实验室实验模拟了使用 CaF_2-CaO-Al_2O_3-MgO-TiO_2 渣系在电渣重熔镍基高温合金 GH8825 过程中 Ti、Si 和 Al 元素的烧损行为（1823 K）。他们将以上反应式（1）和（3）变形，可以得到当温度一定时，合金中元素含量比值与渣中相应氧化物比值的线性关系。结果表明在合金成分一定时，向渣中添加 CaO 可以避免合金中 Ti 元素的烧损；当渣中 CaO 含量较高时，需要向渣中额外添加 TiO_2 避免合金中 Ti 元素的烧损[25]。

可以看到上述热力学分析和实验室研究均在某一个固定的温度下进行的，显然仅在一个固定的温度下进行重熔渣系设计并不能贴合实际生产的情况。除温度之外，合金熔体中元素含量和重熔渣系中各个组元均对目标控制合金元素的含量也存在影响。因此，需要在电极液相线温度至渣/金界面温度范围内，讨论重熔渣系中不同组元、合金成分及温度对钢中目标控制元素的含量进行系统分析。

Duan 等人[27, 34]热力学分析了电渣重熔 Inconel 718 镍基高温合金过程 CaF_2-CaO-Al_2O_3-MgO-TiO_2 渣系对合金中 Al 和 Ti 含量的影响规律。从反应（1）可以得到式(5)，即合金中平衡 Al 含量与渣成分、合金成分以及温度的关系（温度范围：1773 K 至 1973 K）。热力学分析结果表明：重熔渣系对控制合金中 Al 和 Ti 含量的重要程度可以排序为：TiO_2 > Al_2O_3 > CaO > CaF_2 > MgO[27]。1773 K 下渣中 TiO_2 含量 4.26 wt.%时，高温合金中 Al 和 Ti 不再发生烧损，实验结果与理论分析结果一致，说明该热力学分析方法的正确性。

$$\lg[\%\ \mathrm{Al}]=\frac{1}{4}\left\{\lg\frac{a_{\mathrm{R,Al_2O_3}}^{2}}{a_{\mathrm{R,TiO_2}}^{3}}-4\lg f_{\%,\mathrm{Al}}+3\lg f_{\%,\mathrm{Ti}}+3\lg[\%\ \mathrm{Ti}]-\left(\frac{35300}{T}-9.94\right)\right\} \tag{5}$$

电渣重熔过程温度的波动对控制电渣锭中易氧化元素的均匀分布也有重要影响，通过式(5)可以得到温度与合金中 Al 和 Ti 含量的关系。可以看出合金中平衡 Al 与温度呈现正相关，意味着当温度升高时合金中 Ti 比 Al 元素更容易被烧损，因此应向渣中额外添加 TiO_2 防止由于温度升高造成合金中 Ti 元素的烧损。Yang 等人[33]在进行 30 组渣/金平衡实验之后总结出相同的结论。Duan 等人[35]指出渣中 TiO_2 含量为 5 wt.%时，随着 CaO 含量增加合金中 Al 含量增加（如图 1 所示），即渣温较高的情况下造成合金中 Ti 元素的烧损较为严重，此时应当采用的操作是适当降低渣温或者在较高渣温和高 CaO 含量的条件下向渣中添加 TiO_2 也可控制合金中 Al 和 Ti 含量的均匀分布。Hou 等人[28, 36]也报道在较低渣温和低 CaO 含量的 CaF_2-CaO-Al_2O_3-MgO-TiO_2-SiO_2 渣适合重熔 1Cr21Ni5Ti 不锈钢，而在高 CaO 含量的渣中应当伴随着 TiO_2 的加入不仅可以提高电渣锭元素的均匀分布还可以提高电渣锭的纯净度。通过以上结果可知，通过式(5)可全面分析熔渣各个组元以及温度与合金中目标控制元素的关系，然后通过高温实验进一步验证并修正热力学计算结果，能够达到较为准确地获得优化后的渣系成分，该方法也被其他研究者所运用[37-40]。

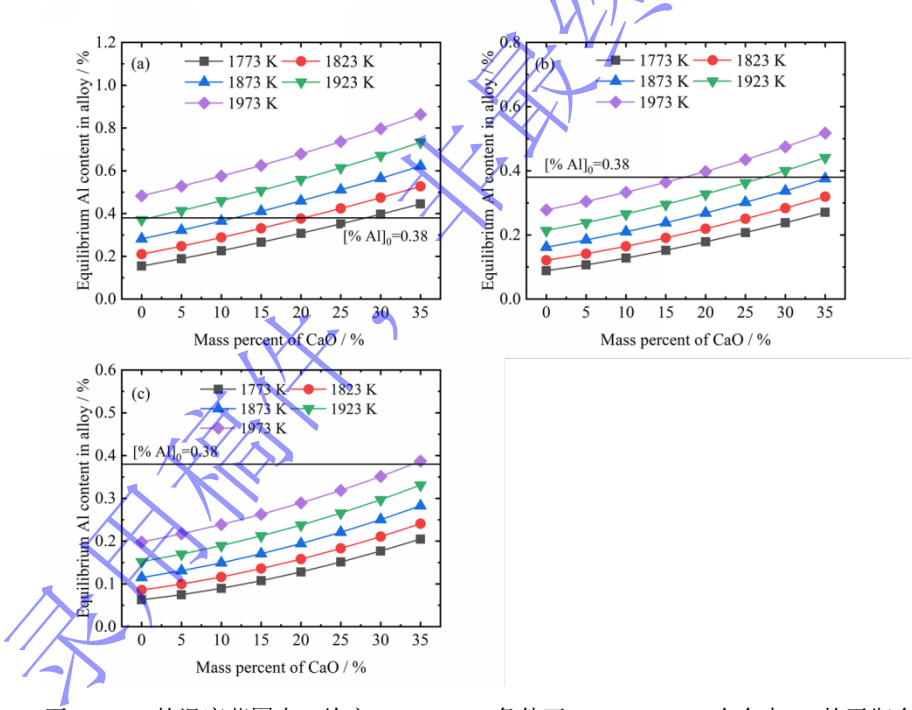

图 1 在 1773 K 至 1973 K 的温度范围内，给定[%Ti] = 1.0 条件下，Inconel 718 合金中 Al 的平衡含量与 CaF_2-CaO-Al_2O_3-MgO-TiO_2 熔渣中 CaO 含量之间的关系：(a) 5 wt.% TiO_2，(b) 10 wt.% TiO_2，(c) 15 wt.% TiO_2[35]。

Fig.1 Relationship between the equilibrium content of Al in the liquid Inconel 718 alloy at a given Ti concentration ([%Ti] = 1.0) and CaO concentration in the CaF_2-CaO-Al_2O_3-MgO-TiO_2 slag over a temperature range of 1773 K to 1973 K: (a) 5 wt.% TiO_2, (b) 10 wt.% TiO_2, (c) 15 wt.% TiO_2.

1.2 电渣重熔含 B、Si 合金渣系成分设计

电渣重熔含硼（B）钢时，如 Cr 含量为 9 ~ 12 wt.%的 9CrMoCoB 耐热钢时，钢中 B 与渣中

SiO_2 反应（如式(6)所示）也会造成电渣锭中 B 和 Si 元素分布不均匀现象[41-45]。

$$4[B]+3(SiO_2)=2(B_2O_3)+3[Si]$$
$$\Delta G_4^{\circ} = -97920 - 91.2T \quad (J\cdot mol^{-1}) \tag{6}$$

Kim 等人[41]通过工业实验研究了改变自耗电极 9CrMoCoB 钢中 Si 元素含量和 CaF_2-CaO-Al_2O_3-B_2O_3-SiO_2 渣中碱度(CaO/SiO_2)对 Si、Mn、Nb 和 B 元素沿电渣锭高度方向分布和纯净度的影响。他们发现增加电极中 Si 含量有助于将电渣锭中 Al 和 Nb 含量控制在目标范围内，高碱度渣有助于降低电渣锭中全氧含量和控制 Si、Mn 和 Nb 含量。但是他们并没有实验测量或理论计算 CaF_2-CaO-Al_2O_3- B_2O_3-SiO_2 渣中渣中 B_2O_3 活度。Peng 等人[42]得到 CaF_2-CaO-MgO-Al_2O_3-B_2O_3-SiO_2 渣中 B_2O_3 活度系数 $\gamma_{B_2O_3}$ 和温度的关系为 $\lg\gamma_{B_2O_3}=-6582/T$，进而发现 55$CaF_2$-20CaO-3MgO-22$Al_2O_3-1B_2O_3-1SiO_2$ 渣（wt.%）适合电渣重熔 9CrMoCoB 耐热钢。Duan 等人[44]使用分子-离子共存理论计算了 1823 K 时 CaF_2-CaO-Al_2O_3-B_2O_3-SiO_2 渣中 B_2O_3 的活度系数为 $\gamma_{B_2O_3}=4.79\times10^{-4}$，该结果略高于 Peng 等人[42]计算结果，这主要由于渣中存在 MgO 所致。通过在 1823 K 至 1973 K 温度范围内，类似于式(5)的处理方法，得到渣中不同组元与钢中平衡 B 含量关系。渣中组元对控制钢中 B 和 Si 元素含量可以排序为 B_2O_3 > SiO_2 > CaO > Al_2O_3 ≅ CaF_2，且钢中平衡 B 含量受温度的影响不大。除了反应(6)之外，钢中 Al 也与渣中 SiO_2 发生如下反应，如式(7)所示。

$$4[Al]+3(SiO_2)=2(Al_2O_3)+3[Si]$$
$$\Delta G_5^{\circ} = -720680 + 133T \quad (J\cdot mol^{-1}) \tag{7}$$

为了把钢中 Al 含量控制在较低水平，则需要将渣中 SiO_2 含量保持在 3.0 wt.%以上。Wang 等人[45]使用实验室级电渣重熔实验发现 47.34CaF_2–20.46CaO–0.5MgO–22Al_2O_3–0.5B_2O_3–9SiO_2 渣可以将 G115 耐热钢中 B 含量控制在 80 ~ 150 ppm 和 Al 含量低于 100 ppm 范围的目标。

1.3 电渣重熔含稀土元素合金渣系成分设计

钢中添加稀土可以起到净化钢液、改善凝固组织、非金属夹杂物改性等作用，从而显著提高钢的力学性能，如提高韧性、耐腐蚀、抗疲劳、耐热等性能等[46, 47]。为了能够在电渣重熔过程中提高钢中稀土元素的收得率，通常在渣池中添加稀土氧化物以抑制稀土元素的烧损。Ren 等人[48]研究 FeCrAl 合金中钇(Y)、镧(La)和铈(Ce)稀土元素在电渣重熔过程的氧化损失行为。造成合金中稀土元素 La 和 Ce 元素的损失可以通过以下化学反应(8)和(9)[49, 50]。他们发现 CaF_2-CaO-Al_2O_3-X (X = Y_2O_3, La_2O_3, Ce_2O_3)渣中稀土氧化物含量和 CaO 的增加，合金中稀土元素含量也会增加，但是渣中 Al_2O_3 含量增加会降低渣中 CaO 的活度，同时使反应(8)和(9)向右移动加剧稀土 La 和 Ce 元素的损失。Duan 等人[26]从热力学角度进一步解释了以上现象，由于 CaF_2-CaO-Al_2O_3-Ce_2O_3 渣中 CaO 含量的增加，使得渣中 Al_2O_3 活度降低和 Ce_2O_3 活度增加，因此可以通过增加渣中 CaO 含量进而抑制稀土 Ce 的烧损，渣中组元对于控制合金中 Ce 的含量作用排序可以为 CaO ≈ Al_2O_3 > Ce_2O_3 (> MgO) > CaF_2。Zhu 等人[51]报道了类似的结果。Wen 等人[50]通过数值模拟的方法揭示了电渣重熔过程中稀土 La 元素的烧损行为，他们发现当金属熔滴穿过渣层过程逐渐发生烧损，实验测得 La 元素的收得

率约为 33.3 %。

$$2[La]+(Al_2O_3)=(La_2O_3)+2[Al]$$
$$\Delta G_6^{o} = -243320 - 49.6T \quad (J\cdot mol^{-1}) \tag{8}$$

$$2[Ce]+(Al_2O_3)=(Ce_2O_3)+2[Al]$$
$$\Delta G_7^{o} = -109330 - 11.1T \quad (J\cdot mol^{-1}) \tag{9}$$

从以上研究结果可知，为了控制电渣锭中合金元素 Al、Ti，Si、B 和稀土元素沿高度方向均匀分布，需要在电渣重熔 CaF_2-CaO-Al_2O_3 基渣系中添加相应合金元素的氧化物，而渣系成分的设计主要依赖于对渣系中组元活度的准确计算。渣中公共组元 CaO 和 Al_2O_3 对控制不同合金元素的作用并不相同。如控制合金中合金元素 Al 和 Ti 时，当渣中添加较高含量的 CaO 时，可以采用低渣温或者向渣中额外添加 TiO_2 以防止合金中 Ti 元素的烧损；当渣中 CaO 含量较低时则需要采用高渣温以防止合金中 Al 元素的烧损。若控制合金中合金元素 Si 和 B 时，增加渣中 CaO 含量，合金中合金元素 B 含量将降低，但是改变渣中 Al_2O_3 含量对控制合金中 B 含量影响不大。若控制合金中稀土元素含量，增加渣中 CaO 含量有利于增加合金中稀土元素的收得率，但是增加渣中 Al_2O_3 含量起相反的作用。因此，除了向 CaF_2-CaO-Al_2O_3 基渣系添加目标合金元素的氧化物外，设计渣中 CaO 和 Al_2O_3 含量也要根据需要控制的合金元素做适当调整。同时，当电渣重熔过程中温度发生波动对合金中不同种类合金元素平衡含量的影响也不尽相同。如温度升高时，相比较 Al 元素，合金中 Ti 元素更加容易被氧化，因此需要在渣中添加 TiO_2 以防止 Ti 元素的烧损。然而，合金中平衡 B（Si）和稀土元素平衡含量对温度的变化并不敏感。因此，只有在充分地分析电渣重熔用渣系每个组元和温度对控制目标元素平衡含量的影响后，再设计合适熔渣成分才可以能够准确地控制电渣锭中目标合金元素的均匀分布。

2 电渣重熔过程易氧化元素控制的动力学

动力学研究可以明确电渣重熔过程中目标控制元素氧化损失反应的限制性环节和在沿电渣锭高度方向的成分变化。表 1 总结了前人在电渣重熔过程动力学方面的研究成果。Wei 等人[52, 53]使用 CaF_2-CaO-Al_2O_3 三元渣系在空气和 Ar 保护气氛下重熔 SAE1020 低碳合金钢（0.19C-0.28Si-0.78Mn-0.13Ni-0.13Cr, wt.%）时认为存在以下四个化学反应[Si]+SiO_2、[Mn]+(MnO)、[Al]+(Al_2O_3)和[Fe]+(FeO)在渣/金界面处同时发生达到总平衡，各个组元在渣相和金属相的传质为限制性环节。根据多相反应动力学的基本方程[24]，熔渣或金属相中的组元 i 的浓度随时间 t 的变化可以表示为：

$$\frac{dC_i}{dt} = k_i \frac{A}{V}(C_i^{*} - C_i) \tag{10}$$

式中：k_i 为组元 i 的传质系数，（$m\cdot s^{-1}$）；A/V 为反应界面与有效熔体体积的比值（“比反应界面”），（m^{-1}）；C_i^{*} 和 C_i 分别为组元 i 在渣-金属界面和渣相或金属相内部的浓度，（$mol\cdot m^{-3}$）。通过获得电极端部、熔滴滴落过程和熔池界面的熔渣和钢液中组元的活度和温度、质量传输系数 k_i 和几何参数 A/V 即可求解电渣重熔过程电渣锭中不同元素含量随铸锭高度方向的变化。根据

Mitchell[19]、Fraser[54]和 Jackson[55]的结果，Wei 等人[52, 53]将渣/金界面的温度在电极端部、金属熔滴和熔池位置分别取为 1540 ℃、1750 ℃和 1695 ℃。熔渣中组元的活度使用 Korousic 和 Holzgruber 报道的模型计算，即熔渣组元 i 的活度系数 γ_i 与摩尔分数 N_i 和温度 T 的关系[56]。铁液中的组元 i 的活度系数 $f_{\%,i}$ 由式(4)计算。铁液中 Si 和 Mn 的扩散系数 D_{Si} 和 D_{Mn}（$\mathrm{m^2\cdot s^{-1}}$）被认为仅仅是温度的函数，即 $D_{\mathrm{Si}}=6.646\times10^{12}\exp(-71123/T)$ 和 $D_{\mathrm{Mn}}=5.973\times10^{10}\exp(-62535/T)$。对铁液中 Al 的扩散系数 D_{Al}，取 $D_{\mathrm{Si}}=D_{\mathrm{Al}}$，但未考虑流体的流动对反应物和生成物在渣相和金属相内的传质系数的影响。结果表明钢中增 Al 主要发生在熔滴位置，但由于熔滴在熔渣停留时间短和其体积较小，对熔渣成分的变化贡献值小于电极端部和金属熔池。

Hou 等人[57, 58]基于薄膜-溶质渗透理论建立了电渣重熔 1Cr21Ni5Ti 不锈钢 Al、Ti 和 Si 元素传质的动力学模型。他们认为在渣/金界面处[Al]+(Al_2O_3)、[Si]+(SiO_2)、[Ti]+(TiO_2)和[Fe]+(FeO)反应达到总热力学平衡。对不同反应位置温度的确定，使用 Thermo-Calc™ 软件计算得到 1Cr21Ni5Ti 不锈钢的熔化温度为 1730 K，根据 Fraser[54]的结果确定电极端部液膜的温度约为 1750 K。渣池与金属熔池界面温度则根据 Dong 等人[59]的结果确定为 1950 K。熔渣中组元活度使用离子-分子共存理论计算得到[60]。根据溶质渗透理论，结合不同反应位置流体流动对传质系数的影响，渣相或金属相中组元 i 的质量传输系数 k_i 的表达式如式(11)所示[24, 61]：

$$k_i=2\sqrt{\frac{D_i}{\pi t_{\mathrm{e}}}}=2\sqrt{\frac{D_i v}{\pi d_{\mathrm{AB}}}} \tag{11}$$

式中：t_{e} 为流体微元在界面处停留时间，它可以表示为每一个微元以相对速度 v 从 A 点到 B 点间的位移 d_{AB} 进行传质。通过测算在电极端部、金属熔滴和金属熔池处金属与渣的相对运动速度分别为 10 $\mathrm{cm\cdot s^{-1}}$、41 $\mathrm{cm\cdot s^{-1}}$ 和 1 $\mathrm{cm\cdot s^{-1}}$，结合文献报道的各个组元的扩散系数 D_i[52, 54]即可得到相应的传质系数 k_i。结果表明电渣重熔 1Cr21Ni5Ti 不锈钢的过程中 Al 在钢液中的传质、SiO_2 在渣中传质以及 Ti 元素在渣和金属相中的传质为反应的限制性环节。Li 等人[62]使用相同的方法建立质量传输模型来描述电渣重熔 G20CrNi2Mo 轴承钢过程钢中溶解氧和 Al 含量的变化，以揭示钢中增氧和 Al 烧损机理。与 Hou 等人[57, 58]不同的是，流体微元在电极端部与熔渣的接触时间 t_{e} 可使用式(11)计算[63]：

$$t_{\mathrm{e}}=3.35\left(\frac{2\pi\cos\theta}{3Q_{\mathrm{m}}}\right)^{\frac{2}{3}}\left(\frac{\mu_{\mathrm{m}}}{g\rho_{\mathrm{m}}\sin\theta}\right)^{\frac{1}{3}}\left(\frac{R_{\mathrm{E}}}{\cos\theta}\right)^{\frac{5}{3}} \tag{12}$$

式中：θ 为电极端部锥角；Q_{m} 为体积熔化速率（$\mathrm{cm^3\cdot s^{-1}}$）；$R_{\mathrm{E}}$ 为自耗电极当量半径；μ_{m} 和 ρ_{m} 是金属熔体的黏度（$\mathrm{Pa\cdot s}$）和密度（$\mathrm{g\cdot cm^{-3}}$）。经过计算得到金属熔滴在电极端部的形成时间约为 2.89 s，而金属熔滴滴落的速度和时间分别为 61 $\mathrm{cm\cdot s^{-1}}$ 和 0.23 s。Li 等人[62]使用电渣重熔工艺优化仿真软件 Meltflow-ESR 分别计算渣池和渣池/金属熔池界面的平均温度分别为 2020 K 和 1957 K。利用以上参数和 Matlab™ 软件可以计算出重熔过程金属熔滴形成、滴落和汇聚在金属熔池的过程，钢中溶解氧[O]和 Al 含量的变化。他们发现金属熔滴脱离电极端部并穿过渣层的过程中，温度急剧增加同时伴随着[O]含量的增加。金属熔滴中[O]含量的增加的限制性环节为渣中 FeO 在渣中的

传质。因此可以通过降低渣池中 FeO 含量，或者降低金属熔滴形成时间和渣池温度可以提高电渣锭的纯净度。史成斌等人[64]建立了使用 CaF_2-CaO-Al_2O_3 渣气氛保护电渣重熔重熔 S316 模具钢，熔渣与钢液间的传氧动力学模型，该模型可以预报渣/钢间传氧方向改变的渣中 FeO 临界含量，并发现随着重熔速率的增加，电极端部钢液向熔渣传氧的速率不断增加。Ju 等人[65]发现电渣重熔 Incoloy825 镍基合金控制 Al、Ti 和 Si 元素时，反应的限制性环节与 Hou 等人[57, 58]的结果一致。Wang 等人[45]对电极端部液膜的表面积 A_{film} 和体积 V_{film} 进行了较为准确的估算，分别使用下式(13)至(15)计算[63]：

$$A_{\text{film}} = \frac{\pi R_{\text{E}}^2}{\cos\theta} \tag{13}$$

$$V_{\text{film}} = \frac{\pi R_{\text{E}}^2 \overline{\delta}}{\cos\theta} \tag{14}$$

$$\overline{\delta} = \left[\frac{3\mu_{\text{m}} Q_{\text{m}}}{2\pi(\rho_{\text{m}} - \rho_{\text{s}}) g \sin\theta \cos\theta} \left(1 - \frac{x^2 \cos^2\theta}{R_{\text{E}}^2} \right) \right]^{\frac{1}{3}} \tag{15}$$

式中：ρ_{s} 是熔渣的黏度密度，（$\text{g}\cdot\text{cm}^{-3}$）；$x$ 是电极端部圆锥部分的高。他们通过建立的传质模型，报道 Ar 气氛保护电渣重熔 G115 耐热钢时，钢中 Al 含量的增加，Si 含量的损失和 B 含量的变化主要发生在电极端部。钢中 B 含量的变化和 Al 含量的增加反应的限制性环节分别为渣中 B_2O_3 的传质和钢中 Al 的传质。重熔渣系 47.34CaF_2-20.46CaO-22Al_2O_3-0.5MgO-9SiO_2-0.5B_2O_3 可以将耐热钢中 B 含量控制在 80 ~150 ppm 和 Al 含量小于 100 ppm 范围之内。部分学者还通过建立数值模型[66-70]和物理模拟[71, 72]对电渣重熔过程的熔池温度场、流场、电磁场分布和凝固过程以及金属熔滴的形成进行详细的分析，对电渣重熔过程有更加深入的认识。从以上研究结果可知，前人对电渣重熔不同反应位置的温度、传质系数和几何参数的优化逐步做了更为准确的估算后，使得传质模型对电渣锭中元素的分布做出更为准确的预报。

表 1 电渣重熔动力学研究工作的总结

Table 1 Summarization of previous research works on the development of mass transfer model for the ESR process

Authors and year	Slag composition	Alloy	Main conclusions	Refs.
Wei et al. 1986	CaF_2-CaO-Al_2O_3	SAE1020 low alloy steel	The increase of Al in the molten steel mainly occurred at the droplet position, but due to the short residence time of the droplet in the slag and its small size, the contribution to the change of the slag composition was smaller than that of the electrode tip and the metal bath.	[52, 53]
Hou et al. 2017	CaO-CaF_2-Al_2O_3-SiO_2-TiO_2-MgO-FeO	1Cr21Ni5Ti stainless steel	The rate-controlling step of the reactions was the mass transfer of Al through the molten steel, SiO_2 through the slag phase, and Ti on both the metal and slag sides.	[57, 58]
Hou et al. 2017	CaO-CaF_2-Al_2O_3-SiO_2-TiO_2-MgO	1Cr21Ni5Ti stainless steel	The rate-controlling step of the desulfurization reaction was the mass transfer in the metal phase, addition of the calcium can enhance the sulfur mass transfer and promote desulfurization during the ESR process.	[73]
Li et al. 2017	CaO-CaF_2-Al_2O_3-SiO_2-MnO-MgO-FeO	G20CrNi2Mo bearing steel	The rate-determining step of [Al] + (FeO) reaction was in the mass transfer of Al in the molten steel. The increase of [O] mainly happened during the formation and falling of metal droplets, which relied on the mass transfer of FeO in the slag phase.	[62]
Hou et al. 2018	CaO-CaF_2-Al_2O_3-SiO_2-TiO_2-MgO	AISI 321 steel	The remelting rate has little effect on the variations of aluminum, titanium, and silicon content in the remelted ingot.	[74]
Duan et al. 2018	CaO-CaF_2-Al_2O_3-TiO_2-MgO	Inconel718 alloy	The mass transfer of TiO_2 and/or Al_2O_3 in the slag phase likely to be the rate-controlling step.	[27]
Duan et al. 2020	CaO-CaF_2-Al_2O_3-TiO_2-MgO	Inconel718 alloy	The interfacial oxygen content increased with increasing temperature, giving rise to a decrease in the desulfurization ratio, and the mass transfer coefficient is $k_{s,m}$=9 ×10^{-4} m/s.	[75]
Wang et al. 2021	CaO-CaF_2-Al_2O_3-MgO	Plain carbon steel	The low content of Al_2O_3 in the slag was beneficial to the removal of aluminum in the steel, while the high content of Al_2O_3 in the slag increased the content of total Al in the steel.	[76]
Ju et al. 2022	CaO-CaF_2-Al_2O_3-SiO_2-TiO_2-MgO-FeO	Incoloy825 alloy	The rate-controlling step of the reactions was the mass transfer of Al through the molten steel, SiO_2 through the slag phase, and Ti on both the metal and slag sides.	[65]
Ju et al. 2022	CaO-CaF_2-Al_2O_3-SiO_2-LiO_2-MgO	Incoloy825 alloy	The rate-controlling step of the reactions was the mass transfer of Al and Ti through the molten steel, and SiO_2 through the slag phase.	[77]
Wang et al. 2023	CaO-CaF_2-Al_2O_3-SiO_2-B_2O_3-MgO-FeO	G115 heat-resistant steel	The rate-determining step for the variation of boron (B) in steel is the mass transfer of B_2O_3 in molten slag, and the mass transfer of Al in liquid steel is the rate-determining for the Al pickup. The pickup of Al, the loss of Si and the variation of B are mainly at the tip of the consumable electrode.	[45]

3 电渣重熔渣系物理化学性质

设计适合的电渣重熔用渣系渣锭的表面质量和凝固组织有着重要影响[6, 78-80]。对于含 TiO_2 渣系，Shi 等人[81]测量了不同 TiO_2 含量对 CaF_2-CaO-Al_2O_3-MgO-TiO_2 渣系黏度和结构的影响，发现随着渣中 TiO_2 含量增加至 9.73 wt.%，熔渣的黏度降低。通过拉曼光谱对熔渣分析结果可知，由于渣中添加 TiO_2 后，渣中$[AlO_4]^{5-}$四面体结构转变为链状 $Ti_2O_6^{4-}$ 结构，降低了熔渣了聚合度，这与测得的黏度降低的实验结果相符。Zheng 等人[82]使用差示扫描量热仪（Differential scanning calorimetry, DSC）测量了不同 TiO_2 含量对 CaF_2-CaO-Al_2O_3-MgO-TiO_2 渣系结晶行为的影响。他们指出当渣中 TiO_2 含量从 4.2 wt.%增加至 16.8 wt.%时，可以降低熔渣结晶速率。当 TiO_2 含量在 4.2 wt.%至 12.6 wt.%的范围内时，熔渣的初生结晶相为 $11CaO{\cdot}7Al_2O_3{\cdot}CaF_2$，继续增加渣中 TiO_2 含量至 16.8 wt.%，结晶相则转变为 $11CaO{\cdot}7Al_2O_3{\cdot}CaF_2$ 和 $CaTiO_3$。该结果说明，由于 CaF_2-CaO-Al_2O_3-MgO-TiO_2 渣中 TiO_2 的加入延缓熔渣的结晶能力，在电渣锭和结晶器间形成薄而均匀的渣层，可以起到润滑作用而且加强电渣锭向水冷结晶器的热量传输，进而提高电渣锭的表面质量和凝固组织。

Shi 等人[83]报道了类似的研究结果，他们在 CaF_2-CaO-Al_2O_3 渣中添加不同含量的 SiO_2，结果表明 SiO_2 添加量在 0 至 6.8 wt.%范围内强烈抑制该渣系的结晶性能，同时随着 SiO_2 含量的增加熔渣的液相线温度也随之降低。考虑到低氟化物渣系可以降低环境污染和电渣重熔过程能源消耗，部分研究者也着手开发低氟化物渣系和研究其物理化学性质与成分的变化关系[84-87]。Shi 等人[85]尝试使

用 Li_2O 代替 CaF_2-CaO-Al_2O_3-MgO 渣系中的 CaF_2，并发现随着 Li_2O 添加量增加至 4.5 wt.%熔渣的黏度降低，这有利于固定式电渣重熔的操作。Zheng 等人[84]继而发现添加碱金属氧化物 Li_2O 能够降低结晶温度从而抑制 CaF_2-CaO-Al_2O_3-MgO-Li_2O 的结晶性能。An 等人[87]通过向 CaF_2-CaO-Al_2O_3-MgO-TiO_2 渣系添加 Na_2O 和 K_2O 后得到类似的结论，并发现 K_2O 起到对熔渣的解聚作用强于 Na_2O。

从表 2 和表 3 可以看出大部分学者改变熔渣某一个成分变量或温度通过实验测量其对熔渣物性参数的影响规律。但是通过实验测量在某一个成分范围内这些物性参数的变化情况将变得十分困难。Yu 等人[88]使用几何模型预报了 1873 K 下 CaF_2-CaO-Al_2O_3 渣的液相区范围内的粘度、电导率和硫容量随熔渣成分的变化，如图 2 所示。结果表明该几何模型计算结果与实验值吻合较好，粘度、电导率和硫容量的预报值与实验结果的偏差分别为 11.0 %, 11.2 % 和 1.7 %。

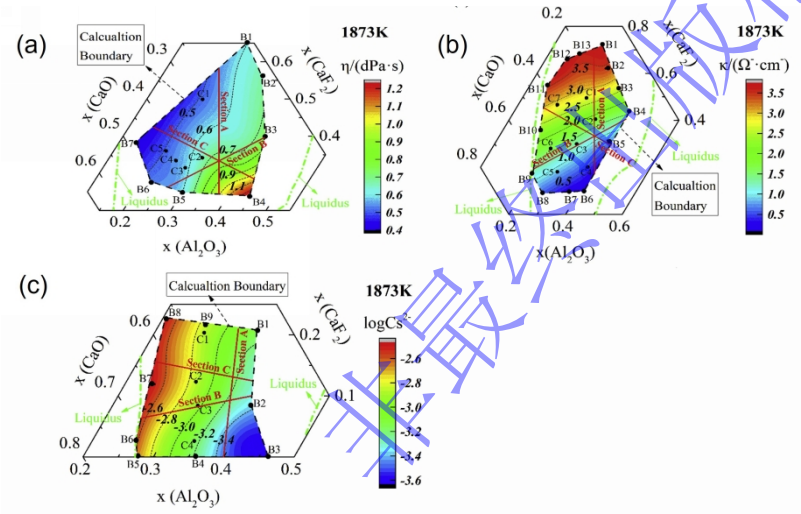

图 2 实验数据和新几何模型计算得出的 CaO–Al_2O_3–CaF_2 渣系在 1873 K 条件下等粘度（a）、等电导率（b）和等硫化物容量等值线[88]

Fig. 2 The experimental data and the calculated iso-viscosity (a), iso-electrical conductivity (b), and iso-sulfide capacity contours of CaO–Al_2O_3–CaF_2 system at 1873 K by the new geometrical model.

近年来，部分学者对含 B_2O_3 电渣重熔渣系的物性参数也进行了研究[89-91]。Geng 等人[89]使用旋转法测量了 55CaF_2–20CaO–3MgO–22Al_2O_3–B_2O_3 渣中添加 0 ~ 3 wt.% B_2O_3 后对熔渣黏度的影响，结果发现渣中添加 2 wt.% B_2O_3 可以使熔渣在较宽温度范围内保持稳定，可以在电渣重熔过程中在铸锭和结晶器之间形成薄而厚度均匀的渣壳。Huang 等人[90]和 Zhang 等人[91]得到类似的结论。对于 CaF_2-CaO-MgO-Al_2O_3-B_2O_3 渣的结晶行为的研究，Peng 等人[92]发现添加 1 wt.% B_2O_3 可以抑制 CaF_2 相的析出，从而获得良好的电渣锭表面质量。通过以上研究结果可知，与 CaF_2-CaO-Al_2O_3-MgO-TiO_2 相比较，含 B_2O_3 精炼渣和保护渣的物性参数研究较为广泛[93-100]，而电渣重熔渣系 CaF_2–CaO–MgO–Al_2O_3–B_2O_3 的物性参数的研究还比较少。Dai 等人[101]发现 CaO-B_2O_3 和 MgO-B_2O_3 二元渣中 B_2O_3 组元会产生挥发现象。Peng 等人[102]使用高温同步热分析仪，以 10 K/min 的升温速率对 55CaF_2-20CaO-3MgO-22Al_2O_3-xB_2O_3 (wt.%, $x \leq$ 3.0)的失重率进行测定，他们发现随着渣中 B_2O_3 含

量大于 0.5 wt.%，通过熔渣的失重率则大幅降低。对于耐热钢中不同 B 元素控制需求，需要在渣中添加的 B_2O_3 含量也不尽相同[44]，在实际电渣重熔过程中由于渣中 CaF_2 和 B_2O_3 的挥发损失对熔渣物性参数的影响仍需要进行研究。

$$3CaF_2 + B_2O_3 = 3CaO + 2BF_3(g) \tag{16}$$

$$CaF_2 + 2BF_3 + 2CaO = 3CaF_2(g) + 2OBF(g) \tag{17}$$

龙鹄等人[103]发现 CaO-Al_2O_3–Ce_2O_3 和 CaO-Al_2O_3–SiO_2-Ce_2O_3 渣中 Ce 离子以正三价形式 Ce^{3+} 稳定存在，两种渣系的熔化温度分别在 1465 ~ 1516 ℃和 1357 ~ 1366 ℃温度范围内，其中 CaO-Al_2O_3–SiO_2-Ce_2O_3 渣的熔化温度随着渣中 Ce_2O_3 含量的增加变化不大。Kitano 等人[104]报道 CaO-Al_2O_3–Ce_2O_3 三元渣系的液相区域（1823 K）位于 $X_{CaO}/X_{Al_2O_3} = 0.8$ 和 $X_{Ce_2O_3} < 0.25$，在 1873 K 下的液相区域则在 $X_{Ce_2O_3} < 0.29$。Guo 等人[105]则发现纯氩气气氛和 1540 ℃条件下 CaO- SiO_2-(Al_2O_3)-CeO_2 渣中 Ce 离子以 Ce^{3+}和 Ce^{4+}混合状态存在，当 CeO_2 含量和 CeO_2/Al_2O_3 增加，熔渣的黏度降低，这主要是因为 CeO_2 的添加可以降低熔渣的聚合能力。Xi 等人[106]指出 CeO_2 光学碱度要高于 CaO 和 BaO，使用含 CeO_2 稀土氧化物渣系有利于锰铁合金的脱磷。Lan 等人[107]构建了等温条件下（1373 K）CaO–SiO_2–CaF_2–Ce_2O_3 渣系相图，根据该四元渣系等温相图可以设计熔渣成分控制结晶相的析出种类，这对于控制电渣锭和结晶器间的渣层传热和润滑性能十分重要[15, 108]。Guo 等人[109]也发现当 CaO-SiO_2-CaF_2-Ce_2O_3 渣中 Ce_2O_3 含量增加，熔渣的熔化性温度逐渐增加，呈现“短渣”性质。而当 Ce_2O_3 含量低于 3 mol%，熔渣在冷却过程中没有发现含稀土的结晶相。

Deng 等人[110]测量了渣中不同 La_2O_3 含量（45、50 和 55 wt.%）对 La_2O_3-SiO_2-Al_2O_3 三元渣系黏度的影响，并发现增加渣中 La_2O_3 含量增加，该三元渣系的黏度降低。Li 等人[111]发现 1723 K 下 CaF_2-CaO-Al_2O_3 渣的挥发产物是 CaF_2 和 AlF_3，随着渣中 La_2O_3 含量的增加，CaF_2 和 AlF_3 的饱和蒸气压逐渐降低，因此减少了 CaF_2-CaO-Al_2O_3-La_2O_3 渣的挥发损失；并且随着 La_2O_3 降低熔渣的结晶温度，进而抑制 CaF_2 和 $11CaO \cdot 7Al_2O_3 \cdot CaF_2$ 结晶相的析出。

表 2 电渣重熔用 CaF_2-CaO-Al_2O_3 基渣系物理化学性质研究工作的总结

Table 2 Summarization of previous research works on the physicochemical properties of the CaF_2-CaO-Al_2O_3-based ESR-type slag

Authors and year	Slag composition	Research contents	Refs.
Wang et al. 2013	CaF_2-CaO-Al_2O_3-SiO_2	The effects of CaF_2 content and temperature on the physical properties, such as melting temperature and electrical conductivity of the slag were investigated.	[112]
Dong et al. 2015	CaF_2-CaO-Al_2O_3	The water-cooling tube method was adopted to measure the thermal conductivity of solid fluoride slag.	[113]
Shi et al. 2015	CaF_2-CaO-Al_2O_3-(SiO_2)	The crystallization characteristics of the slags with varying amounts of SiO_2 were experimentally studied.	[83]
Shi et al. 2016	CaF_2-CaO-Al_2O_3-MgO-Li_2O	The effect of the substitution of CaF_2 with Li_2O on the viscosity and structure of the low-fluoride slag was studied.	[85]
Zheng et al. 2016	CaF_2-CaO-Al_2O_3-MgO-TiO_2	The crystallization characteristics of the slags with various TiO_2 contents were studied using a single hot thermocouple technique, SEM-EDS, and X-ray diffraction.	[114]
Liu et al. 2018	CaF_2-CaO-Al_2O_3	The slags with varying CaO/Al_2O_3 mass ratio and CaF_2 content were selected for investigating the vaporization behavior of slag by thermo gravimetry and ion and molecule coexistence theory.	[115]
Shi et al. 2018	CaF_2-CaO-Al_2O_3-MgO-TiO_2	The effects of TiO_2 contents on the melting point, viscosity, density, optical alkalinity, electrical conductivity, and other physical parameters of the slag were studied.	[116]
Lao et al. 2019	CaF_2-CaO-SiO_2	Effects of the basicity (CaO/SiO_2) and the CaF_2 content on the viscosity of the slag were investigated by the rotating cylinder method in temperatures ranging from 1773 to 1533 K.	[117]
Yu et al. 2019	CaF_2-CaO-Al_2O_3	An extended geometrical model is introduced for the prediction of the viscosity, electrical conductivity, and sulfide capacity of the slag.	[88]
Ju et al. 2020	CaF_2-CaO-Al_2O_3-MgO-Li_2O-TiO_2	The evaporation of fluoride from the slag with different TiO_2 contents was investigated.	[86]
Zheng et al. 2020	CaF_2-CaO-Al_2O_3-MgO-TiO_2	The crystallization kinetics and structure of the slag for electroslag remelting (ESR) were investigated by differential scanning calorimetry and Raman spectroscopy, respectively.	[82]
Ju et al. 2021	CaF_2-CaO-Al_2O_3-MgO-TiO_2	The relationship between the viscosity and structure of the slag with different CaF_2 contents and CaO/Al_2O_3 ratios was studied using the rotating cylinder method, Fourier transform infrared spectroscopy, and Raman spectrometry.	[118]
Geng et al. 2022	CaF_2-CaO-Al_2O_3-MgO-B_2O_3	The effects of the B_2O_3 content on slag viscosity, breakpoint temperature, and activation energy for viscous flow were investigated.	[89]
Hou et al. 2022	CaF_2-CaO-Al_2O_3-MgO-TiO_2	The melting temperature of the slag systems and thermodynamic equilibrium between A-286 superalloy and the slag were experimentally carried out based on the phase diagram, FactSage™, and thermodynamic calculation.	[11]
Wan et al. 2022	CaF_2-CaO-Al_2O_3-B_2O_3-SiO_2-Li_2O	The structure and viscosity of the slag with varying CaF2 and Li2O contents were investigated by Raman spectroscopy, ^{27}Al, ^{29}Si and ^{11}B magic angle spinning nuclear magnetic resonance (MASNMR) spectroscopy, and rotating cylinder method, respectively.	[119]
An et al. 2023	CaF_2-CaO-Al_2O_3-MgO-TiO_2-(Na_2O-K_2O)	The non-isothermal evaporation of the low-fluoride slag is studied using thermogravimetric analysis.	[87]
Huang et al. 2023	CaF_2-CaO-Al_2O_3-MgO-SiO_2-B_2O_3	The effect of SiO_2 and B_2O_3 on viscosity and surface tension of the slag.	[90]
Yang et al. 2023	CaF_2–Al_2O_3–TiO_2	The microstructure of the ESR slag under an electric field was investigated by employing the molecular dynamics simulation.	[120]
Ju et al. 2024	CaF_2–CaO–Al_2O_3–SiO_2–MgO–TiO_2	The electrical conductivity and viscosity of the slag system with different CaO/Al_2O_3 (0.9–1.8) were measured by a high-temperature physical property measuring instrument, and the structure of the slag was analyzed by FTIR and Raman spectroscopy.	[14]
Zhang et al. 2024	CaF_2-CaO-Al_2O_3-MgO-B_2O_3	The melting temperature, electrical conductivity, and viscosity of the slag were determined.	[91]

表 3 含稀土氧化物电渣重熔用渣系物理化学性质的研究工作的总结

Table 3 Summarization of previous research works on the physicochemical properties of the ESR-type slag containing rare earth oxides

Authors and year	Slag composition	Research contents	Refs.
Long et al. 2010	$CaO-Al_2O_3–SiO_2-Ce_2O_3$ $CaO-Al_2O_3-Ce_2O_3$	The change of melting temperature and viscosity of the slag with increasing Ce_2O_3 content in the slag.	[103]
Kitano et al. 2016	$CaO-Al_2O_3-Ce_2O_3$	The phase equilibria and activities of CaO, Al_2O_3, and Ce_2O_3 in the system at 1 823 and 1 873 K were investigated by using a chemical equilibration technique.	[104]
Deng et al. 2016	$La_2O_3-SiO_2-Al_2O_3$	The viscosities and free-running temperatures of the slag system were measured using an internal rotating cylinder method	[110]
Qi et al. 2017	$CaO-Al_2O_3-Li_2O-Ce_2O_3$	The 45 g of slag and 120 g of steel were charged into the magnesia crucible and then placed into the vacuum induction furnace at 1873 K.	[121]
Guo et al. 2020	$CaO–SiO_2-(Al_2O_3)-CeO_2$	The effect of the CeO_2 content and CeO_2/Al_2O_3 ratio on the melt viscosity of the slag was determined using the rotating cylinder method.	[105]
Ma et al. 2020	$CaO-SiO_2-Nb_2O_5-CeO_2-CaF_2$	The effect of Nb_2O_5 and basicity on the viscosity of the slag system was studied from 1653 to 1813 K in reducing atmosphere by rotating cylinder method.	[122]
She et al. 2020	$CaO–SiO_2–CaF_2–La_2O_3$	The crystallization behaviors of the slag with different basicity have been studied by differential scanning calorimetry (DSC), field emission scanning electron microscopy (SEM) and X-ray diffraction (XRD).	[123]
Guo et al. 2021	$CaO–SiO_2(–Al_2O_3)–La_2O_3$	The effects of La_2O_3 and the La_2O_3/Al_2O_3 ratios on the melt viscosity of the slag at high temperatures using the rotating cylinder method.	[124]
Lan et al. 2021	$CaO–SiO_2–CaF_2–Ce_2O_3$	The isothermal phase diagram of the slag was constructed, and the phase equilibria data of REEs in REE-bearing slag were provided.	[107]
Zheng et al. 2021	$CaO-Al_2O_3-Ce_2O_3$	The iso-activity curves of oxides in the ternary systems were estimated at 1500 ℃, 1550 ℃, and 1600 ℃, respectively.	[125]
Lan et al. 2022	$CaO–SiO_2–CaF_2–Ce_2O_3$	The viscosity of RE-bearing slag and kinetics for nucleation and growth of RE-phase were studied.	[126]
Li et al. 2022	$CaF_2–CaO–Al_2O_3–(La_2O_3)$	The vaporization and crystallization of the slags with different La_2O_3 contents for electroslag remelting were investigated.	[111]
Zheng et al. 2022	$CaO–Al_2O_3–Ce_2O_3–MgO–SiO_2$	The effect of Ce_2O_3 content on the properties (melting point and viscosity) and structure of the slag was analyzed.	[127]
Zheng et al. 2022	$CaO–Al_2O_3–Ce_2O_3–MgO–SiO_2$	The properties and structure of the slag with different CaO/Al_2O_3 were investigated by hemispherical melting point method, the rotating cylinder method, and Raman spectroscopy, respectively.	[128]
Zhao et al. 2023	$CaO-Al_2O_3-SiO_2$.MgO-CeO_2	Effect of CeO_2 Content on melting temperature and mineral-phase structure of the slag using the thermogravimetric analysis (TG) and differential scanning calorimetry (DSC) methods.	[129]
Guo et al. 2024	$CaO-SiO_2-CaF_2-Ce_2O_3$	The effects of Ce_2O_3 and CaF_2 on viscosity and structure of the slag	[109]
Wang et al. 2024	$CaO-Al_2O_3-MgO-SiO_2-Ce_2O_3$	The impact of Ce_2O_3 content on the crystalline phase and structure within the slag was studied.	[130]
Li et al. 2024	$CaF_2-CaO-Al_2O_3-MgO-Ce_2O_3$	The influence of Ce_2O_3 addition on the variation of the melting properties of the slag system was studied.	[131]

电渣重熔具有较高的去除夹杂物和脱硫的能力[10, 13, 132]，这是由于电渣重熔夹杂物的去除主要发生在电极端部位置[133]，此处与熔渣的接触面积大，加之电渣重熔渣系具有较高的碱度和较好的流动性。张立峰等人[134]提出夹杂物容量概念以描述夹杂物向渣中的溶解速率，如式(18)所示：

$$Zh = \frac{g \cdot \rho_{\text{slag}}^2 \cdot (C_{i,\text{saturation}} - C_i) \cdot d_{\text{p},0}^3}{\eta_{\text{slag}}^2} \tag{18}$$

式中：C_i 和 $C_{i,\text{saturation}}$ 分别表示渣中含有夹杂物相 i 的质量分数和渣中该物相 i 的饱和质量分数（wt. %）；$d_{\text{p},0}$ 为夹杂物初始直径（m）；ρ_{slag} 和 η_{slag} 分别代表熔渣的密度（$\text{kg}\cdot\text{m}^{-3}$）和动力学粘度（$\text{kg}\cdot\text{m}^{-1}\cdot\text{s}^{-1}$）；$g$ 为重力常数（$\text{m}\cdot\text{s}^{-2}$）。从式中可以看出，较高的浓度差 $(C_{i,\text{saturation}} - C_i)$ 和较低的熔渣黏度 η_{slag} 有利于钢中非金属夹杂物的去除。

优化渣系的物性参数对电渣重熔操作和电渣锭质量有着重要的影响，同时实验测量以上不同 CaF_2-CaO-Al_2O_3 基渣系中 Al_2O_3、TiO_2、SiO_2、B_2O_3 以及稀土氧化物的活度对于控制电渣锭中合金元素的均匀化分布也十分的重要，但是相关的研究却十分的匮乏。Zheng 等人[125]通过计算 CaO-Al_2O_3-Ce_2O_3 三元渣中形成的不同复杂化合物的热力学参数，如形成焓、形成熵和等压热熔，进一步得到 CaO-Al_2O_3-Ce_2O_3 三元渣在 1773 K、1823 K 以及 1873 K 条件下每个组元的等活度线。随着对环境保护的重视程度原来越高，电渣重熔渣系低氟化设计，如降低渣中 CaF_2 含量或向渣中添加

碱金属氧化物，也逐渐受到越来越多的关注[15]。低 CaF_2 含量渣系中组元活度的准确测量或计算，重熔过程元素烧损反应热力学、动力学以及渣系物性参数还需要进一步研究。

4 结论和展望

(1) 电渣重熔过程易氧化元素的控制主要依赖于含氟渣系和钢液中组元活度的准确计算。使用离子-分子共存理论能够较为准确低计算含 CaF_2 重熔渣系中组元的活度。对于控制钢中不同种类的易氧化元素，通常需要加入适量的对应元素的氧化物，但是对于 CaF_2-CaO-Al_2O_3 基重熔渣系中的公共组元 CaO 和 Al_2O_3 对不同元素的作用并不相同。对控制钢中 Al 和 Ti 含量来讲，增加渣中 CaO 含量导致钢中 Ti 烧损和 Al 含量的增加，因此还需要额外增加 TiO_2 以抑制钢中 Ti 元素的烧损；对控制钢中 Si 和 B 含量，渣中加入 CaO 会导致钢中 B 含量的烧损，但是改变 Al_2O_3 含量却对钢中 B 含量影响不大；对控制钢中稀土元素 Ce 和 La 含量，增加渣中 CaO 含量有利于提高稀土元素的收得率，渣中 Al_2O_3 却起到相反的作用。反应温度对不同元素的控制也有不同的影响，相比较 Al 元素在高渣温条件下 Ti 元素更加容易烧损，因此需要向渣中添加一定量的 TiO_2，但是温度的升高对钢中 B 含量和稀土元素的含量影响不大。在电渣重熔温度范围内，通过分析渣系各个组元对钢中目标控制元素含量分析，可以做到对钢中元素的控制的准确渣系成分设计。

(2) 电渣重熔过程传质模型预报结果的准确性依赖于熔渣和钢液中组元的热力学活度、不同反应位置温度（电极端部、金属熔滴、渣池和金属熔池界面）、传质系数和几何参数的准确性。电渣重熔含 Al 和 Ti 不锈钢和镍基合金时，氧化反应的限制性环节为 Al 在钢液中的传质、SiO_2 在渣中传质以及 Ti 元素在渣和金属相中的传质为反应的限制性环节；对于含 Si 和 B 耐热钢时，限制性环节为渣中 B_2O_3 的传质和钢中 Al 的传质。相比较热力学，动力学研究还不充分，主要因为不同重熔操作和钢种会导致渣池和金属熔池流场和温度场分布也不尽相同，因此氧化反应的限制行环节还需要进一步的研究。

(3) 适合的重熔渣系成分设计不仅对控制钢中易氧化元素的均匀分布十分重要，对重熔渣系的物性参数也有重要的影响，因为适合的熔渣成分可以降低电渣重熔过程的能源消耗，还可以提高电渣锭表面质量和凝固组织。对含 TiO_2、B_2O_3 和稀土氧化物的 CaF_2-CaO-Al_2O_3 重熔渣系的物性参数的研究主要集中在黏度和结晶性能的研究上。重熔渣系中组元 TiO_2、B_2O_3 和稀土氧化物的活度的实验室测量还未见报道。开发低氟渣也越来越受关注，相对应的元素氧化热力学、动力学和熔渣物性参数也应该进一步的研究。

参 考 文 献

[1] Jiang Z H, Dong Y W, Geng X, et al. *Electroslag Metallurgy* [M]. Beijing: Science Press, 2015.
(姜周华, 懂艳伍, 耿鑫, 等. 电渣冶金学 [M]. 北京: 科学出版社, 2015.)

[2] Zhang L F, Zhu M Y. *Metallurgy of Steelmaking* [M]. Beijing: Higher Education Press, 2023.
(张立峰, 朱苗勇. 炼钢学 [M]. 北京: 高等教育出版社, 2023.)

[3] Shi C-B, Wang S-J, Li J, et al. Non-metallic inclusions in electroslag remelting: A review [J]. *J. Iron Steel Res. Int.*,

2021, 28(12): 1483. https://doi.org/10.1007/s42243-021-00700-4.

[4] Wen T J, Ren Q, Zhang L F, et al. Evolution of nonmetallic inclusions during the electroslag remelting process [J]. *Steel Res. Int.*, 2021, 92(6). https://doi.org/10.1002/srin.202000629.

[5] Duan S, Lee M J, Su Y, et al. Evolution of nonmetallic inclusions in 80-t 9CrMoCoB large-scale ingots during electroslag remelting process [J]. *Int. J. Miner., Metall. Mater.*, 2024, 31(7): 1525. https://doi.org/10.1007/s12613-024-2905-9.

[6] Li Z B. *Electroslag Metallurgy Theory and Practice* [M]. Beijing: Metallurgical Industry Press, 2010.
(李正邦. 电渣冶金的理论与实践 [M]. 北京: 冶金工业出版社, 2010.)

[7] Jiang Z H, Dong Y W, Geng X, et al. Development and application of electroslag remeltingtechnology for high quality special steels [J]. *Iron Steel*, 2023, 58(9): 15. https://doi.org/10.13228/j.boyuan.issn0449-749x.20230253.
(姜周华, 董艳伍, 耿鑫, 等. 高品质特殊钢电渣重熔技术的开发和应用 [J]. 钢铁, 2023, 58(9): 15.)

[8] Wen T J. *Study on Flow Phenomena of Molten Steel and Behavior of Non-Metallic Inclusions During Electroslag Remelting* [Dissertation]. Beijing: University of Science and Technology Beijing, 2021.
(文甜洁. 电渣重熔过程钢液流动现象和非金属夹杂物行为的研究 [学位论文]. 北京: 北京科技大学, 2021)

[9] Reyes-Carmona F, Mitchell A. Deoxidation of ESR slags [J]. *ISIJ Int.*, 1992, 32(4): 529. https://doi.org/10.2355/isijinternational.32.529.

[10] Shi C. Deoxidation of electroslag remelting (ESR) – A review [J]. *ISIJ Int.*, 2020, 60(6): 1083. https://doi.org/10.2355/isijinternational.ISIJINT-2019-661.

[11] Hou D, Wang D, Zhou X, et al. Study on physical and chemical properties of slag used for electroslag remelting of superalloy containing titanium and aluminum [J]. *Metall. Mater. Trans. B*, 2022, 53(5): 2972. https://doi.org/10.1007/s11663-022-02579-2.

[12] Tommaney J W, Andolina P S, Buri R C. *Method and means of reducing the oxidization of reactive elements in an electroslag remelting operation*: United States Patent, US4953177A. 1990-8-28.

[13] Duan S C, Shi X, Wang F, et al. A review of methodology development for controlling loss of alloying elements during the electroslag remelting process [J]. *Metall. Mater. Trans. B*, 2019, 50(6): 3055. https://doi.org/10.1007/s11663-019-01665-2.

[14] Ju J, He K, Qiu G, et al. Effect of CaO/Al_2O_3 on electrical conductivity, viscosity and structure of electroslag remelting-type TiO_2-bearing slag [J]. *Ironmaking Steelmaking*, 2024. https://doi.org/10.1177/03019233241238580.

[15] Duan S C, Guo H J. The methodology development for improving energy utilization and reducing fluoride pollution of the electroslag remelting process: A review [J]. *Steel Res. Int.*, 2020, 91(7): 1900634. https://doi.org/10.1002/srin.201900634.

[16] Polishko G, Stovpchenko G, Medovar L, et al. Physicochemical comparison of electroslag remelting with consumable electrode and electroslag refining with liquid metal [J]. *Ironmaking Steelmaking*, 2018, 46(8): 789. https://doi.org/10.1080/03019233.2018.1428419.

[17] Shi C, Zheng D, Guo B, et al. Evolution of oxide–sulfide complex inclusions and its correlation with steel cleanliness during electroslag rapid remelting (ESRR) of tool steel [J]. *Metall. Mater. Trans. B*, 2018, 49(6): 3390. https://doi.org/10.1007/s11663-018-1398-1.

[18] Liu F-B, Gao J-Z, Cao H-B, et al. Effect of slag composition on elements oxidation behavior of GH984G superalloy for electroslag remelting withdrawal process [J]. *J. Iron Steel Res. Int.*, 2022, 29(5): 761. https://doi.org/10.1007/s42243-021-00602-5.

[19] Mitchell A, Joshi S. The thermal characteristics of the electroslag process [J]. *Metall. Trans.*, 1973, 4(3): 631. https://doi.org/10.1007/BF02643068.

[20] Wang F, Tan J, Liu Z, et al. Effect of dynamic formation of multiphase slag skin on heat transfer and magneto-hydrodynamic flow in electroslag remelting process [J]. *J. Mater. Res. Technol.*, 2023, 25: 1696.

https://doi.org/10.1016/j.jmrt.2023.06.042.

[21] Schneider R, Wiesinger V, Gelder S, et al. Effect of different remelting parameters on slag temperature and energy consumption during ESR [J]. *ISIJ Int.*, 2022, 62(6): 1199. https://doi.org/10.2355/isijinternational.ISIJINT-2021-498.

[22] Chen C X, Gao R F, Zhao W X. Effect of slag composition on Mg, Al or Ti content in Ni-based superalloy during ESR [J]. *Acta Metall. Sin.*, 1984, 20(3): 243.
(陈崇禧, 高荣富, 赵文祥. 熔渣成分对电渣重熔 Ni 基高温合金中 Mg, Al, Ti 含量的影响 [J]. 金属学报, 1984, 20(3): 243.)

[23] Pateisky G, Biele H, Fleischer H J. The reactions of titanium and silicon with Al_2O_3-CaO-CaF_2 slags in the ESR process [J]. *J. Vac. Sci. Technol.*, 1972, 9(6): 1318. https://doi.org/10.1116/1.1317029.

[24] Guo H J. *Metallurgical Physical Chemistry* [M]. 2nd ed. Beijing: Metallurgical Industry Press, 2013.
(郭汉杰. 冶金物理化学教程 [M]. 第二版. 北京: 冶金工业出版社, 2013.)

[25] Jiang Z H, Hou D, Dong Y W, et al. Effect of slag on titanium, silicon, and aluminum contents in superalloy during electroslag remelting [J]. *Metall. Mater. Trans. B*, 2016, 47(2): 1465. https://doi.org/10.1007/s11663-015-0530-8.

[26] Duan S C, Park J H. Comparison of oxidation behavior of various reactive elements in alloys during electroslag remelting (ESR) process: An overview [J]. *ISIJ Int.*, 2022, 62(8): 1561. https://doi.org/10.2355/isijinternational.ISIJINT-2022-015.

[27] Duan S, Shi X, Mao M, et al. Investigation of the oxidation behaviour of Ti and Al in Inconel 718 superalloy during electroslag remelting [J]. *Sci. Rep.*, 2018, 8(1): 5232. https://doi.org/10.1038/s41598-018-23556-3.

[28] Hou D, Jiang Z, Dong Y, et al. Thermodynamic design of electroslag remelting slag for high titanium and low aluminium stainless steel based on IMCT [J]. *Ironmaking Steelmaking*, 2016, 43(7): 517. https://doi.org/10.1080/03019233.2015.1110920.

[29] Wagner C, Elliott J F. *The Physical Chemistry of Steelmaking* [M]. New York: Wiley and Sons, 1958.

[30] Shen Z, Guo J, Duan S, et al. Thermodynamics and optimization of a slag system for Al and Ti burning loss control of a Φ1100-mm Ni-based superalloy ingot during the electroslag remelting process [J]. *JOM*, 2023, 75(7): 2636. https://doi.org/10.1007/s11837-023-05807-5.

[31] Ju J, Zhu Z, Yang K, et al. Control of Al and Ti contents during electroslag remelting of high-temperature Ni-based alloys [J]. *Rare Met. Mater. Eng.*, 2021, 50(10): 3550.

[32] Chen C X, Wang Y, Fu J, et al. A study on the titanium loss during electroslag remelting high titaium and low aluminum content superalloy [J]. *Acta Metall. Sin.*, 1981, 17(1): 50.
(陈崇禧, 王涌, 傅杰, 等. 高钛低铝高温合金电渣重熔中钛烧损的研究 [J]. 金属学报, 1981, 17(1): 50.)

[33] Yang J G, Park J H. Distribution behavior of aluminum and titanium between nickel-based alloys and molten slags in the electro slag remelting (ESR) process [J]. *Metall. Mater. Trans. B*, 2017, 48(4): 2147. https://doi.org/10.1007/s11663-017-0994-9.

[34] Duan S C, Guo H J, Shi X, et al. Thermodynamic analysis of the smelting of Inconel 718 superalloy during electroslag remelting process [J]. *Chin. J. Eng.*, 2018, 40(S1): 53. https://doi.org/10.13374/j.issn2095-9389.2018.s1.009.
(段生朝, 郭汉杰, 石骁, 等. Inconel 718 高温合金电渣重熔热力学分析 [J]. 工程科学学报, 2018, 40(S1): 53.)

[35] Duan S C, Lee M J, Kim D S, et al. Effect of temperature on the oxidation behavior of Al and Ti in Inconel® 718 alloy by ESR slag with different amounts of CaO [J]. *JOM*, 2022, 74(3): 1228. https://doi.org/10.1007/s11837-021-05139-2.

[36] Hou D, Jiang Z-H, Qu T-P, et al. Aluminum, titanium and oxygen control during electroslag remelting of stainless steel based on thermodynamic analysis [J]. *J. Iron Steel Res. Int.*, 2019, 26(1): 20. https://doi.org/10.1007/s42243-018-0107-2.

[37] Ju J T, Yang K S, Ji K H, et al. Thermodynamic study on design of electroslag remelting slag for Incoloy 825 Alloy

[J]. *Chin. J. Eng.*, 2020, 42(S1): 119. https://doi.org/10.13374/j.issn2095-9389.2020.03.07.s01.
(巨建涛, 杨康帅, 棘广恒, 等. Incoloy825 合金电渣重熔低氟渣系设计的热力学研究 [J]. 工程科学学报, 2020, 42(S1): 119.)

[38] Yin B, Li W M, Wu S P, et al. Thermodynamic analysis of Al and Ti element loss inelectroslag remelting Inconel718 superalloy [J]. *Iron Steel*, 2019, 54(5): 86. https://doi.org/10.13228/j.boyuan.issn0449-749x.20180378.
(尹彬, 李万明, 吴少鹏, 等. Inconel718 高温合金电渣重熔铝钛元素烧损热力学分析 [J]. 钢铁, 2019, 54(5): 86.)

[39] Shen Z M, Guo J, Duan S C, et al. Thermodynamic model for Al and Ti burning control of GH4706 large size electroslag ingot GH4706 [J]. *J. Iron Steel Res.*, 2021, 33(9): 901. https://doi.org/10.13228/j.boyuan.issn1001-0963.20210091.
(沈中敏, 郭靖, 段生朝, 等. 大尺寸电渣锭铝钛烧损控制的热力学模型 [J]. 钢铁研究学报, 2021, 33(9): 901.)

[40] Liu F-B, Zhang H-B, Gao J-Z, et al. Thermodynamic analysis of aluminum and titanium oxidation during electroslag remelting process of Inconel 625 alloy [J]. *J. Northeast. Univ. (Nat. Sci.)*, 2022, 43(5): 652. https://doi.org/10.12068/j.issn.1005-3026.2022.05.007.
(刘福斌, 张海宝, 高俊哲, 等. 电渣重熔 Inconel 625 合金铝钛氧化的热力学分析 [J]. 东北大学学报(自然科学版), 2022, 43(5): 652.)

[41] Kim D S, Lee G J, Lee M B, et al. Manufacturing of 9CrMoCoB steel of large ingot with homogeneity by ESR process [Z]. IOP Conference Series: Materials Science and Engineering. IOP Publishing. 2016: 12002. https://doi.org/10.1088/1757-899x/143/1/012002.

[42] Peng L, Jiang Z, Geng X. Design of ESR slag for remelting 9CrMoCoB steel through experiments and thermodynamic calculations [J]. *Calphad*, 2020, 70: 101782. https://doi.org/10.1016/j.calphad.2020.101782.

[43] Peng L, Jiang Z, Geng X. Reaction mechanisms between molten CaF_2-based slags and molten 9CrMoCoB steel [J]. *Int. J. Miner., Metall. Mater.*, 2020, 27(5): 611. https://doi.org/10.1007/s12613-020-1976-5.

[44] Duan S C, Lee M J, Kim D S, et al. Oxidation behavior of boron in 9CrMoCoB steel by CaF_2-CaO-Al_2O_3-SiO_2-B_2O_3 electroslag remelting (ESR) type slag [J]. *J. Mater. Res. Technol.*, 2022, 17: 574. https://doi.org/10.1016/j.jmrt.2022.01.033.

[45] Wang S, Shi C, Liu Z, et al. Active element variation of G115 heat-resistant steel and its dependence on slag composition during electroslag remelting [J]. *J. Mater. Res. Technol.*, 2023, 23: 6176. https://doi.org/10.1016/j.jmrt.2023.02.191.

[46] Dong H, Lian X T, Hu C D, et al. High performance steels: The scenario of theory and technology [J]. *Acta Metall. Sin.*, 2020, 56(4): 558. https://doi.org/10.11900/0412.1961.2020.00058.
(董瀚, 廉心桐, 胡春东, 等. 钢的高性能化理论与技术进展 [J]. 金属学报, 2020, 56(4): 558.)

[47] Wang X, Wu Z, Li B, et al. Inclusions modification by rare earth in steel and the resulting properties: A review [J]. *J. Rare Earths*, 2023. https://doi.org/10.1016/j.jre.2023.04.015.

[48] Ren Y, Zhang L, Yu L, et al. Yield of Y, La, Ce in high temperature alloy during electroslag remelting process [J]. *Metall. Res. Technol.*, 2016, 113(4): 405. https://doi.org/10.1051/metal/2016017.

[49] Karasev A, Suito H. Quantitative evaluation of inclusion in deoxidation of Fe-10 mass pct Ni alloy with Si, Ti, Al, Zr, and Ce [J]. *Metall. Mater. Trans. B*, 1999, 30(2): 249. https://doi.org/10.1007/s11663-999-0054-1.

[50] Wen T, Zhang H, Li X, et al. Numerical simulation on the oxidation of lanthanum during the electroslag remelting process [J]. *JOM*, 2018, 70(10): 2157. https://doi.org/10.1007/s11837-018-3049-z.

[51] Zhu J, Zheng D, Liu M, et al. Thermodynamic analysis of the oxidation behavior of cerium in high-speed steel during electroslag remelting [J]. *Steel Res. Int.*, 2024: 2300824. https://doi.org/10.1002/srin.202300824.

[52] Wei J H, Mitchell A. Changes in composition during AC ESR. I. Theoretical development [J]. *Acta Metall. Sin.*, 1984, 20(5): b261.
(魏季和, Mitchell A. 交流电渣重熔过程中的成分变化-I.理论传质模型 [J]. 金属学报, 1984, 20(5): b261.)

[53] Wei J H, Mitchell A. Changes in composition during A.C. ESR-II. laboratory results and analysis [J]. *Acta Metall. Sin.*, 1984, 20(5): 406.
(魏季和, Mitchell A. 交流电渣重熔过程中的成分变化-II. 实验室试验结果及分析 [J]. 金属学报, 1984, 20(5): 406.)

[54] Fraser M E, Mitchell A. Mass transfer in the electroslag process. Part1: Mass-transfer model [J]. *Ironmaking Steelmaking*, 1976, 3(5): 279.

[55] Jackson R O. Study of thermal instabilities in electroslag melting [D]. Vancouver: University of British Columbia, 1972.

[56] Korousic B, Holzgruber W. Über die oxidationsgleichgewichte beim elektro-schlacke-umschmelzen [J]. *Berg-Huettenmaenn. Monatsh.*, 1977, 122(7): 287.

[57] Hou D, Jiang Z H, Dong Y W, et al. Effect of slag composition on the oxidation kinetics of alloying elements during electroslag remelting of stainless steel: Part-2 control of titanium and aluminum content [J]. *ISIJ Int.*, 2017, 57(8): 1410. https://doi.org/10.2355/isijinternational.ISIJINT-2017-148.

[58] Hou D, Jiang Z H, Dong Y W, et al. Effect of slag composition on the oxidation kinetics of alloying elements during electroslag remelting of stainless steel: Part-1 mass-transfer model [J]. *ISIJ Int.*, 2017, 57(8): 1400. https://doi.org/10.2355/isijinternational.ISIJINT-2017-147.

[59] Dong Y W, Jiang Z H, Fan J X, et al. Comprehensive mathematical model for simulating electroslag remelting [J]. *Metall. Mater. Trans. B*, 2016, 47(2): 1475. https://doi.org/10.1007/s11663-015-0546-0.

[60] Zhang J. *Computational Thermodynamics of Metallurgical Melts and Solutions* [M]. Beijing: Metallurgical Industry Press, 2007.
(张鉴. 冶金熔体和溶液的计算热力学 [M]. 北京: 冶金工业出版社, 2007.)

[61] Hou D. *Metallurgical Reaction and Aloying Elements Control during Electroslag Remelting of Stainless Steel Containing Aluminum and Titainum* [Dissertation]. Shenyang: Northeastern University, 2017.
(侯栋. 电渣重熔含铝钛不锈钢的冶金反应和成分控制研究 [学位论文]. 沈阳: 东北大学, 2017)

[62] Li S, Cheng G, Miao Z, et al. Kinetic analysis of aluminum and oxygen variation of G20CrNi2Mo bearing steel during industrial electroslag remelting process [J]. *ISIJ Int.*, 2017, 57(12): 2148. https://doi.org/10.2355/isijinternational.ISIJINT-2017-227.

[63] Etienne M. Loss of reactive elements during electroslag processing of iron-base alloys [D]. Vancouver: University of British Columbia, 1970.

[64] Shi C B, Guo H J, Chen X C, et al. Kinetic study of oxygen transfer during protective gas electroslag remelting process [J]. *Spec. Steel*, 2013, 34(2): 11.
(史成斌, 郭汉杰, 陈希春, 等. 气体保护电渣重熔过程氧传递的动力学研究 [J]. 特殊钢, 2013, 34(2): 11.)

[65] Ju J, Li Q, Zhu Z, et al. Kinetic study of control of alloy elements during electroslag remelting of Incoloy825 [J]. *Metall. Res. Technol.*, 2022, 119(4): 418. https://doi.org/10.1051/metal/2022047.

[66] Wang F, Xiong Y, Li B, et al. A sequence-coupled mathematical model of magneto-hydrodynamic two-phase flow and heat transfer in a triplex-electrode electroslag remelting furnace [J]. *Steel Res. Int.*, 2019, 90(6): 1800481. https://doi.org/10.1002/srin.201800481.

[67] Wang Q, Cai H, Pan L p, et al. Numerical investigation of influence of electrode immersion depth on heat transfer and fluid flow in electroslag remelting process [J]. *JOM*, 2016, 68(12): 3143. https://doi.org/10.1007/s11837-016-2021-z.

[68] Wang Q, Qi F, Wang F, et al. Numerical investigation on electromagnetism and heat transfer in electroslag remelting process with triple-electrode [J]. *Int. J. Precis. Eng. Manuf.*, 2015, 16(12): 2467. https://doi.org/10.1007/s12541-015-0317-5.

[69] Wang Q, Zhao R, Fafard M, et al. Three-dimensional magnetohydrodynamic two-phase flow and heat transfer

analysis in electroslag remelting process [J]. *Appl. Therm. Eng.*, 2015, 80: 178. https://doi.org/10.1016/j.applthermaleng.2014.12.075.

[70] Kharicha A, Karimi-Sibaki E, Wu M, et al. Review on modeling and simulation of electroslag remelting [J]. *Steel Res. Int.*, 2018, 89(1): 1700100. https://doi.org/10.1002/srin.201700100.

[71] Wang H, Zhong Y, Li Q, et al. Visualization study on the droplet evolution behaviors in electroslag remelting process by superimposing a transverse static magnetic field [J]. *ISIJ Int.*, 2016, 56(2): 255. https://doi.org/10.2355/isijinternational.ISIJINT-2015-581.

[72] Wang H, Zhong Y, Li Q, et al. Effect of current frequency on droplet evolution during magnetic-field-controlled electroslag remelting process via visualization method [J]. *Metall. Mater. Trans. B*, 2017, 48(1): 655. https://doi.org/10.1007/s11663-016-0779-6.

[73] Hou D, Jiang Z-H, Dong Y-W, et al. Mass transfer model of desulfurization in the electroslag remelting process [J]. *Metall. Mater. Trans. B*, 2017, 48(3): 1885. https://doi.org/10.1007/s11663-017-0921-0.

[74] Hou D, Liu F-B, Qu T-P, et al. Behavior of alloying elements during drawing-ingot-type electroslag remelting of stainless steel containing titanium [J]. *ISIJ Int.*, 2018, 58(5): 876. https://doi.org/10.2355/isijinternational.ISIJINT-2017-687.

[75] Duan S C, Shi X, Zhang M C, et al. Effect of slag composition on the deoxidation and desulfurization of Inconel 718 superalloy by ESR type slag without deoxidizer addition [J]. *Metall. Mater. Trans. B*, 2020, 51(1): 353. https://doi.org/10.1007/s11663-019-01729-3.

[76] Wang J, Zhang L, Wen T, et al. Kinetic prediction for the composition of inclusions in the molten steel during the electroslag remelting [J]. *Metall. Mater. Trans. B*, 2021, 52(3): 1521. https://doi.org/10.1007/s11663-021-02120-x.

[77] Ju J, Zhu Z, An J, et al. Kinetic study on the reaction between Incoloy 825 alloy and low-fluoride slag for electroslag remelting [J]. *Green Process. Synth.*, 2022, 11(1): 1. https://doi.org/doi:10.1515/gps-2022-0001.

[78] Schneider R, Wiesinger V, Gelder S, et al. Effect of the slag composition on the process behavior, energy consumption, and nonmetallic inclusions during electroslag remelting [J]. *Steel Res. Int.*, 2023, 94(4): 2200483. https://doi.org/10.1002/srin.202200483.

[79] Mills K C, Keene B J. Physicochemical properties of molten CaF_2 -based slags [J]. *Int. Met. Rev.*, 1981, 26(1): 21. https://doi.org/10.1179/imtr.1981.26.1.21.

[80] Li X, Geng X, Jiang Z H, et al. Influences of slag system on metallurgical quality for high temperature alloy by electroslag remelting [J]. *Iron Steel*, 2015, 50(9): 41. https://doi.org/10.13228/j.boyuan.issn0449-749x.20140719.
(李星, 耿鑫, 姜周华, 等. 电渣重熔高温合金渣系对冶金质量的影响 [J]. 钢铁, 2015, 50(9): 41.)

[81] Shi C-B, Zheng D-L, Shin S-H, et al. Effect of TiO_2 on the viscosity and structure of low-fluoride slag used for electroslag remelting of Ti-containing steels [J]. *Int. J. Miner., Metall. Mater.*, 2017, 24(1): 18. https://doi.org/10.1007/s12613-017-1374-9.

[82] Zheng D, Shi C, Li J, et al. Crystallization kinetics and structure of CaF_2–CaO–Al_2O_3–MgO–TiO_2 slag for electroslag remelting [J]. *ISIJ Int.*, 2020, 60(3): 492. https://doi.org/10.2355/isijinternational.ISIJINT-2019-461.

[83] Shi C-B, Li J, Cho J-W, et al. Effect of SiO_2 on the crystallization behaviors and in-mold performance of CaF_2-CaO-Al_2O_3 slags for drawing-ingot-type electroslag remelting [J]. *Metall. Mater. Trans. B*, 2015, 46(5): 2110. https://doi.org/10.1007/s11663-015-0402-2.

[84] Zheng D, Li J, Shi C. Development of low-fluoride slag for electroslag remelting: Role of Li_2O on the crystallization and evaporation of the slag [J]. *ISIJ Int.*, 2020, 60(5): 840. https://doi.org/10.2355/isijinternational.ISIJINT-2019-575.

[85] Shi C-B, Shin S-H, Zheng D-L, et al. Development of low-fluoride slag for electroslag remelting: Role of Li_2O on the viscosity and structure of the slag [J]. *Metall. Mater. Trans. B*, 2016, 47(6): 3343. https://doi.org/10.1007/s11663-016-0826-3.

[86] Ju J-T, Ji G-H, An J-L, et al. Effect of TiO_2 on fluoride evaporation from CaF_2–CaO–Al_2O_3–MgO–Li_2O–(TiO_2) slag

[J]. *Ironmaking Steelmaking*, 2020, 48(1): 109. https://doi.org/10.1080/03019233.2020.1737792.

[87] An B, Gu Y, Ju J, et al. Fluoride evaporation of low-fluoride CaF_2-CaO-Al_2O_3-MgO-TiO_2-(Na_2O-K_2O) slag for electroslag remelting [J]. *Materials*, 2023, 16(7): 2777. https://doi.org/10.3390/ma16072777.

[88] Yu Z, Leng H, Luo Q, et al. Geometrical modelling of the physicochemical properties of CaO–Al_2O_3–CaF_2 slag at 1873K [J]. *Ceram. Int.*, 2019. https://doi.org/10.1016/j.ceramint.2019.12.033.

[89] Geng X, Tao X-R, Jiang Z-H, et al. Effect of B_2O_3 on ESR slag viscosity for remelting 9CrMoCoB steel [J]. *ISIJ Int.*, 2022, 62(6): 1070. https://doi.org/10.2355/isijinternational.ISIJINT-2021-470.

[90] Huang Y, Shi C-B, Wan X-X, et al. Viscosity and surface tension of CaF_2–CaO–Al_2O_3-based slag with varying SiO_2 and B_2O_3 contents for ESR of rotor steel [J]. *J. Iron Steel Res. Int.*, 2023, 30(1): 74. https://doi.org/10.1007/s42243-022-00861-w.

[91] Zhang Y-J, Kong L-Z, Zang X-M, et al. Study on properties of CaF_2–CaO–Al_2O_3–MgO–B_2O_3 electroslag remelting slag for rack plate steel [J]. *High Temp. Mater. Processes*, 2024, 43(1): 20220316. https://doi.org/10.1515/htmp-2022-0316.

[92] Peng L, Jiang Z, Geng X, et al. Effect of B_2O_3 on the crystallization behavior of CaF_2-based slag for electroslag remelting 9CrMoCoB steel [J]. *Metals*, 2019, 9(12): 1331. https://doi.org/10.3390/met9121331.

[93] Shu Q, Wang Z, Klug J L, et al. Effects of B_2O_3 and TiO_2 on crystallization behavior of slags in Al_2O_3-CaO-MgO-Na_2O-SiO_2 system [J]. *Steel Res. Int.*, 2013, 84(11): 1138. https://doi.org/10.1002/srin.201200341.

[94] Yan P, Nie P, Huang S, et al. Sulphide capacity and mineralogy of BaO and B_2O_3 modified CaO–Al_2O_3 top slag [J]. *ISIJ Int.*, 2014, 54(7): 1570. https://doi.org/10.2355/isijinternational.54.1570.

[95] Wang L, Cui Y, Yang J, et al. Melting properties and viscosity of SiO_2-CaO-Al_2O_3-B_2O_3 system [J]. *Steel Res. Int.*, 2015, 86(6): 670. https://doi.org/10.1002/srin.201400353.

[96] Shu Q, Li P, Zhang X, et al. Thermodynamics and structure of CaO-Al_2O_3-3 Mass Pct B_2O_3 slag at 1773 K (1500 °C) [J]. *Metall. Mater. Trans. B*, 2016, 47(6): 3527. https://doi.org/10.1007/s11663-016-0781-z.

[97] Shi Y, Wei Y, Zhou S, et al. Effect of B_2O_3 content on the viscosity of copper slag [J]. *J. Alloys Compd.*, 2020, 822: 153478. https://doi.org/10.1016/j.jallcom.2019.153478.

[98] Wang H, Zhang T, Zhu H, et al. Effect of B_2O_3 on melting temperature, viscosity and desulfurization capacity of CaO–based refining flux [J]. *ISIJ Int.*, 2011, 51(5): 702. https://doi.org/10.2355/isijinternational.51.702.

[99] Wang W, Cai D, Zhang L. A review of fluorine-free mold flux development [J]. *ISIJ Int.*, 2018, 58(11): 1957. https://doi.org/10.2355/isijinternational.ISIJINT-2018-232.

[100] Xu J F, Chen D, Weng W P, et al. Evaluation of surface tension for MgO-B_2O_3-SiO_2-FeO boron-rich slag [J]. *J. Cent. South Univ. (Sci. Technol.)*, 2017, 48(6): 1413. https://doi.org/10.11817/j.issn.1672-7207.2017.06.001.
(许继芳，陈栋，翁文凭，等. 富硼渣 MgO-B_2O_3-SiO_2-FeO 体系表面张力计算 [J]. 中南大学学报(自然科学版), 2017, 48(6): 1413.)

[101] Dai C, Zhang X, Shui L. A new method for measuring activities in slags containing a volatile component [J]. *Metall. Mater. Trans. B*, 1995, 26(3): 651. https://doi.org/10.1007/BF02653887.

[102] Peng L, Jiang Z, Geng X. Effect of B_2O_3 on the evaporation behavior of the CaF_2-based slag for electroslag remelting the COST-FB2 steel [J]. *J. Mater. Metall.*, 2020, 19(1): 26. https://doi.org/10.14186/j.cnki.1671-6620.2020.01.005.
(彭雷朕，姜周华，耿鑫. B_2O_3 对电渣重熔冶炼 COST-FB2 钢用 CaF_2 基熔渣挥发性能的影响 [J]. 材料与冶金学报, 2020, 19(1): 26.)

[103] Long H, Cheng G G, Wu B, et al. Melting and fluidity properties of refining slag containing Ce_2O_3 for steelmaking [J]. *J. Chin. Rare Earth Soc.*, 2010, 28(6): 721.
(龙鹄，成国光，吴彬，等. 含 Ce_2O_3 炼钢精炼渣熔化及流动特性的研究 [J]. 中国稀土学报, 2010, 28(6): 721.)

[104] Kitano R, Ishii M, Uo M, et al. Thermodynamic properties of the CaO–$AlO_{1.5}$–$CeO_{1.5}$ system [J]. *ISIJ Int.*, 2016, 56(11): 1893. https://doi.org/10.2355/isijinternational.ISIJINT-2016-201.

[105] Guo W, Wang Z, Zhao Z, et al. Effect of CeO_2 on the viscosity and structure of high-temperature melt of the CaO-SiO_2(-Al_2O_3)-CeO_2 system [J]. *J. Non-Cryst. Solids*, 2020, 540: 120085. https://doi.org/10.1016/j.jnoncrysol.2020.120085.

[106] Xi X, Luo D, Cai X, et al. Dephosphorisation of ferromanganese alloy using rare earth oxide-containing slags [J]. *Can. Metall. Q.*, 2018, 57(4): 493. https://doi.org/10.1080/00084433.2018.1501142.

[107] Lan X, Gao J, Li Y, et al. Thermodynamics and kinetics of REEs in CaO–SiO_2–CaF_2–Ce_2O_3 system: A theoretical basis toward sustainable utilization of REEs in REE-Bearing slag [J]. *Ceram. Int.*, 2021, 47(5): 6130. https://doi.org/10.1016/j.ceramint.2020.10.192.

[108] Zheng L, Peng B, Li Y, et al. Compositional optimization of ESR slags for H13 steel containing Ce and Mg [J]. *Metall. Mater. Trans. B*, 2023, 54(6): 3312. https://doi.org/10.1007/s11663-023-02909-y.

[109] Guo W, Liu X, Liu F, et al. Effect of Ce_2O_3 and CaF_2 on viscosity and structure of CaO-SiO_2-CaF_2-Ce_2O_3 slag [J]. *J. Rare Earths*, 2024. https://doi.org/10.1016/j.jre.2024.04.015.

[110] Deng Y-C, Wu S-L, Jiang Y-J, et al. Study on viscosity of the La_2O_3-SiO_2-Al_2O_3 slag system [J]. *Metall. Mater. Trans. B*, 2016, 47(4): 2433. https://doi.org/10.1007/s11663-016-0711-0.

[111] Li T, Li G, Zhang Z, et al. Fluoride vaporization and crystallization of CaF_2–CaO–Al_2O_3–(La_2O_3) slag for vacuum electroslag remelting [J]. *Vacuum*, 2022, 196: 110807. https://doi.org/10.1016/j.vacuum.2021.110807.

[112] Wang X, Li Y, Yan C, et al. The physical properties of slags for electro-slag remelting in CaF_2-CaO-Al_2O_3-SiO_2 system [J]. *J. Manuf. Sci. Prod.*, 2013, 13(1-2): 73. https://doi.org/10.1515/jmsp-2012-0025.

[113] Dong Y, Jiang Z, Cao Y, et al. Effective thermal conductivity of slag crust for ESR slag [J]. *ISIJ Int.*, 2015, 55(4): 904. https://doi.org/10.2355/isijinternational.55.904.

[114] Zheng D L, Li J, Shi C B, et al. Effect of TiO_2 on the crystallisation behaviour of CaF_2–CaO–Al_2O_3–MgO slag for electroslag remelting of Ti-containing tool steel [J]. *Ironmaking Steelmaking*, 2016, 45(2): 135. https://doi.org/10.1080/03019233.2016.1248699.

[115] Liu Y, Zhang Z, Li G, et al. Investigation of fluoride vaporization from CaF_2-CaO-Al_2O_3 slag for vacuum electroslag remelting [J]. *Vacuum*, 2018, 158: 6. https://doi.org/10.1016/j.vacuum.2018.09.027.

[116] Shi S, Geng X, Jiang Z-H, et al. Influence of TiO_2 content on the physical properties of the CaF_2-Al_2O_3-CaO-MgO-TiO_2 five yuan electroslag remelting system [J]. *Chin. J. Eng.*, 2018, 40(S1): 47. https://doi.org/10.13374/j.issn2095-9389.2018.s1.008.
(师帅，耿鑫，姜周华，等. TiO_2 含量对于 CaF_2-Al_2O_3-CaO-MgO-TiO_2 五元电渣重熔渣系物性参数的影响 [J]. 工程科学学报, 2018, 40(S1): 47.)

[117] Lao Y, Gao Y, Deng F, et al. Effects of basicity and CaF_2 on the viscosity of CaF_2–CaO–SiO_2 slag for electroslag remelting process [J]. *Metall. Res. Technol.*, 2019, 116(6): 638. https://doi.org/10.1051/metal/2019066.

[118] Ju J-T, Yang K-S, Zhu Z-H, et al. Effect of CaF_2 and CaO/Al_2O_3 on viscosity and structure of TiO_2-bearing slag for electroslag remelting [J]. *J. Iron Steel Res. Int.*, 2021, 28(12): 1541. https://doi.org/10.1007/s42243-021-00683-2.

[119] Wan X, Shi C, Zhao Y, et al. Effect of CaF_2 and Li_2O on structure and viscosity of low-fluoride slag for electroslag remelting of rotor steel [J]. *J. Non-Cryst. Solids*, 2022, 597: 121914. https://doi.org/10.1016/j.jnoncrysol.2022.121914.

[120] Yang P, Liang X, Lu D, et al. Molecular dynamics simulations of electroslag remelting slag under electric field: CaF_2-Al_2O_3-TiO_2 [J]. *Metall. Mater. Trans. B*, 2023, 55(1): 565. https://doi.org/10.1007/s11663-023-02977-0.

[121] Qi J, Liu C, Zhang C, et al. Effect of Ce_2O_3 on structure, viscosity, and crystalline phase of CaO-Al_2O_3-Li_2O-Ce_2O_3 slags [J]. *Metall. Mater. Trans. B*, 2017, 48(1): 11. https://doi.org/10.1007/s11663-016-0850-3.

[122] Ma Z, Zhao Z, Guo W, et al. Influence of Nb_2O_5 and basicity on the viscosity and structure of CaO-SiO_2-Nb_2O_5-CeO_2-CaF_2 slag system [J]. *Metall. Res. Technol.*, 2020, 117(3): 307. https://doi.org/10.1051/metal/2020023.

[123] She X, An Z, Zhang Z, et al. Crystallization behavior of synthesized CaO–SiO_2–CaF_2–La_2O_3 rare earth-containing slag [J]. *ISIJ Int.*, 2020, 60(5): 832. https://doi.org/10.2355/isijinternational.ISIJINT-2019-557.

[124] Guo W, Ding Z, Wang J, et al. Effect of La_2O_3 on the viscosity and structure of CaO–SiO_2(–Al_2O_3)–La_2O_3 melts [J]. *Mater. Chem. Phys.*, 2021, 266: 124526. https://doi.org/10.1016/j.matchemphys.2021.124526.

[125] Zheng X, Liu C. Thermodynamic properties assessment of CaO-Al_2O_3-Ce_2O_3 system [J]. *Metall. Mater. Trans. B*, 2021, 52(5): 3183. https://doi.org/10.1007/s11663-021-02245-z.

[126] Lan X, Gao J, Wang Z, et al. Viscosity of RE-bearing slag systems and kinetics of nucleation and growth for RE-phases [J]. *Ceram. Int.*, 2022, 48(9): 13304. https://doi.org/10.1016/j.ceramint.2022.01.209.

[127] Zheng X, Liu C. Effect of Ce_2O_3 on the melt structure and properties of CaO–Al_2O_3-based slag [J]. *ISIJ Int.*, 2022, 62(6): 1091. https://doi.org/10.2355/isijinternational.ISIJINT-2021-545.

[128] Zheng X, Liu C. Investigation of CaO/Al_2O_3 mass ratio on the properties and structure of Ce_2O_3-Containing CaO–Al_2O_3-based tundish flux [J]. *ISIJ Int.*, 2022, 62(3): 418. https://doi.org/10.2355/isijinternational.ISIJINT-2021-438.

[129] Zhao B, Wu W, Zhi J, et al. Effect of CeO_2 content on melting performance and microstructure of CaO-Al_2O_3-SiO_2-MgO refining slag [J]. *Metals*, 2023, 13(1): 179. https://doi.org/10.3390/met13010179.

[130] Wang L, Zhu H, Chen J, et al. Effect of Ce_2O_3 content on structure, viscosity, and melting properties of CaO-Al_2O_3-MgO-SiO_2-Ce_2O_3 slag [J]. *Ironmaking Steelmaking*, 2024. https://doi.org/10.1177/03019233241254237.

[131] Li S S, Chen Y X, Zang X M, et al. Effect of Ce_2O_3 on melting behavior of CaF_2-CaO-Al_2O_3-MgO for electroslag remelting slag [J]. *Iron Steel*, 2024, 59(3): 117. https://doi.org/10.13228/j.boyuan.issn0449-749x.20230443.
(李世森, 陈宇新, 臧喜民, 等. Ce_2O_3 对 CaF_2-CaO-Al_2O_3-MgO 电渣重熔渣系熔化行为的影响 [J]. 钢铁, 2024, 59(3): 117.)

[132] Shi C B, Huang Y, Zhang J X, et al. Review on desulfurization in electroslag remelting [J]. *Int. J. Miner., Metall. Mater.*, 2021, 28(1): 18. https://doi.org/10.1007/s12613-020-2075-3.

[133] Fu J, Zhu J. Changes in oxide inclusions during electroslag remelting [J]. *Acta Metall. Sin.*, 1964, 7(3): 250.
(傅杰, 朱觉. 电渣重熔过程中氧化物夹杂的变化 [J]. 金属学报, 1964, 7(3): 250.)

[134] Zhang L F, Ren Y. Concept of inclusion capacity of slag and its application [J]. *Iron Steel*, 2023, 58(2): 47. https://doi.org/10.13228/j.boyuan.issn0449-749x.20220407.
(张立峰, 任英. 精炼渣的夹杂物容量的概念及其应用 [J]. 钢铁, 2023, 58(2): 47.)